Photonics-Based Microwave Frequency Mixing: Methodology and Applications

*Zhenzhou Tang, Yifei Li, Jianping Yao, and Shilong Pan**

Photonics-based microwave frequency mixing provides distinct features in terms of wide frequency coverage, broad instantaneous bandwidth, small frequency-dependent loss, and immunity to electromagnetic interference as compared with its electronic counterpart, which can be a key technical enabler for future broadband and multifunctional RF systems. Herein, all-optical and optoelectronic microwave frequency mixing techniques are reviewed, with an emphasis on the latest advances in photonics-based microwave frequency mixers with improved performance in terms of conversion efficiency, dynamic range, mixing-spur suppression, mixing functionality, and polarization independence. Innovative applications enabled by photonics-based microwave frequency mixers, such as radio-over-fiber communication systems, radar systems, satellite payloads and electronic warfare systems, are also reviewed. In addition, efforts in implementing integrated photonics-based microwave mixers that lead to a dramatic reduction in size, weight, and power consumption are also reviewed.

1. Introduction

Although it is hard to pinpoint the exact time of the invention of the first microwave mixer, it is widely believed that frequency mixers already existed 100 years ago due to the invention of heterodyne and super-heterodyne receivers.[1] Since then, as one of the most essential and fundamental functionalities, frequency mixers are widely adopted in most of the microwave and millimeter-wave systems, such as radars, wireless communications systems, electronic warfare (EW) systems, and microwave instruments. For example, in a wireless communication system, as illustrated in **Figure 1**, a low-frequency intermediate-frequency (IF) signal is upconverted to the high-frequency radio frequency (RF) band by a frequency mixer operating in upconversion mode for free-space transmission, while the received RF signal is downconverted by another mixer at the receiver working in downconversion mode to the IF band so that it can be filtered using fixed IF passband filters to increase the selectivity. Without doubt, the bandwidth, conversion efficiency, dynamic range, and mixing-spur level of a frequency mixer significantly influences the performance of a microwave system.

In principle, frequency mixing can be regarded as a nonlinear process, by which new frequency components are created. If two input signals, denoted as $V_{\mathrm{LO}}\sin\omega_{\mathrm{LO}}t$ and $V_{\mathrm{RF}}\sin\omega_{\mathrm{RF}}t$, are applied to a frequency mixer, the signal at the output can be written as

$$V_{\mathrm{LO}}\sin\omega_{LO}t \times V_{\mathrm{RF}}\sin\omega_{\mathrm{RF}}t = \frac{V_{\mathrm{LO}}\times V_{\mathrm{RF}}}{2}[\cos(\omega_{\mathrm{LO}}-\omega_{\mathrm{RF}})t - \cos(\omega_{\mathrm{LO}}+\omega_{\mathrm{RF}})t] \quad (1)$$

that is, two frequency components, the sum and difference frequencies, are generated. However, this ideal frequency mixing can never be achieved in the real world. Take a most widely used electrical mixer based on a diode as an example, the current–voltage (*I*–*V*) relationship of a diode is typically given by[2]

$$i = a_0 + a_1 v + a_2 v^2 + a_3 v^3 + \cdots \quad (2)$$

where a_{n} are the Taylor coefficients. When the two input signals are combined and applied to the diode, that is, $v = V_{\mathrm{LO}}\sin\omega_{\mathrm{LO}}t + V_{\mathrm{RF}}\sin\omega_{\mathrm{RF}}t$, the signal at the output, when ignoring the third- and higher-order mixing components, is expressed as

$$\begin{aligned} i = {} & \underbrace{a_2 V_{\mathrm{LO}} V_{\mathrm{RF}}\left[\cos\left(\omega_{\mathrm{LO}}-\omega_{\mathrm{RF}}\right)t-\cos\left(\omega_{\mathrm{LO}}+\omega_{\mathrm{RF}}\right)t\right]}_{\text{Frequency-converted terms}} + \underbrace{a_0+\frac{1}{2}a_2V_{\mathrm{LO}}^2+\frac{1}{2}a_2V_{\mathrm{RF}}^2}_{\text{DC terms}} \\ & + \underbrace{\left(a_1V_{\mathrm{LO}}+\frac{3}{4}a_3V_{\mathrm{LO}}^3+\frac{3}{2}a_3V_{\mathrm{LO}}V_{\mathrm{RF}}^2\right)\sin\omega_{\mathrm{LO}}t+\left(a_1V_{\mathrm{RF}}+\frac{3}{4}a_3V_{\mathrm{RF}}^3+\frac{3}{2}a_3V_{\mathrm{LO}}^2V_{\mathrm{RF}}\right)\sin\omega_{\mathrm{RF}}t}_{\text{LOandRFleakages}} \\ & \underbrace{-\frac{1}{2}a_2V_{\mathrm{LO}}^2\cos2\omega_{\mathrm{LO}}t-\frac{1}{2}a_2V_{\mathrm{RF}}^2\cos2\omega_{\mathrm{RF}}t-\frac{1}{4}a_3V_{\mathrm{LO}}^3\cos3\omega_{\mathrm{LO}}t-\frac{1}{4}a_3V_{\mathrm{RF}}^3\cos3\omega_{\mathrm{RF}}t+\cdots}_{\text{Harmonics of the inputs}} \\ & \underbrace{-\frac{3}{4}\left[a_3V_{\mathrm{LO}}^2V_{\mathrm{RF}}\cos\left(2\omega_{\mathrm{LO}}+\omega_{\mathrm{RF}}\right)t-\cos\left(2\omega_{\mathrm{LO}}-\omega_{\mathrm{RF}}\right)t\right]-\frac{3}{4}a_3V_{\mathrm{LO}}V_{\mathrm{RF}}^2\cos\left(\omega_{\mathrm{LO}}\pm2\omega_{\mathrm{RF}}\right)t+\cdots}_{\text{Intermodulation products}} \end{aligned} \quad (3)$$

Dr. Z. Tang, Prof. S. Pan
Key Laboratory of Radar Imaging and Microwave Photonics, Ministry of Education
Nanjing University of Aeronautics and Astronautics
Nanjing 210016, China
E-mail: pans@nuaa.edu.cn
Prof. Y. Li
University of Massachusetts at Dartmouth
North Dartmouth MA 02747, USA
Prof. J. Yao
University of Ottawa
Ottawa K1N 6N5 Canada

The ORCID identification number(s) for the author(s) of this article can be found under https://doi.org/10.1002/lpor.201800350

DOI: 10.1002/lpor.201800350

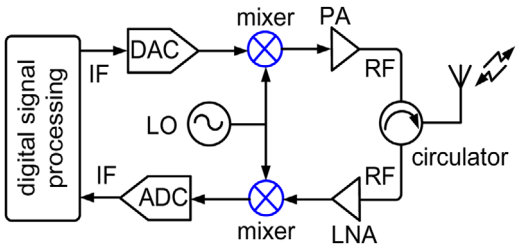

Figure 1. Mixers in wireless communication systems. DAC: digital-to-analog converter; ADC: analog-to-digital converter; PA: power amplifier; LNA: low noise amplifier; LO: local oscillator.

As can be seen from Equation (3), except for the desired frequency-converted components, other unwanted terms (LO/RF leakage, high-order harmonics, and intermodulation products), regarded as mixing spurs, are created. These components can be observed from the signal at the output of any electrical mixer. For instance, **Figure 2**a shows a picture of a commercially available broadband mixer (Marki M9-0440) where the key parameters are included, and Figure 2c illustrates the electrical spectrum of a converted signal when a 20-GHz RF and a 19-GHz LO are applied to the input of the mixer. As can be seen, apart from the desired 1-GHz tone, a large number of unwanted frequency components are generated, although the nominal RF/LO bandwidth of the mixer is 4–44 GHz and the IF bandwidth is DC to 3 GHz. The undesired mixing spurs restrict the operational bandwidth as well as the dynamic range of the mixer, which is one of the most important reasons why most of today's RF systems still have to employ multi-stage narrow-band frequency converters (together with bandpass filters) to ensure a sufficiently high dynamic range, favorable conversion efficiency, and acceptable mixing-spur suppression.

Recently, the fast development of high-speed wireless communications,[3] internet of things (IoT),[4] high-resolution/multifunctional radars,[5] and software-defined satellite payloads[6] has driven the demand for mixers with higher performances. Photonics-based microwave frequency mixing that has the potential to provide high mixing performance has been considered a solution and has attracted significant interest. **Figure 3** illustrates a general system architecture for a photonics-based microwave mixer, which consists of an electrical-to-optical (E–O) conversion module, an optical processing unit, and an optical-to-electrical (O–E) conversion component. Photonics-based microwave mixing can be implemented either in the E–O conversion, the optical processor (if all-optical nonlinear devices such as semiconductor optical amplifiers or highly nonlinear fibers [HNLFs] are employed), and the O–E conversion stage. Thanks to the distinct features offered by photonic technologies in terms of broad instantaneous bandwidth, low loss, light weight, flat frequency response, favorable isolation, and immunity to electromagnetic interference (EMI), performing frequency mixing in the optical domain facilitates a net gain in instantaneous bandwidth, frequency range, port-to-port isolation, and transmission efficiency. In addition, because of the well-known wavelength-division multiplexing (WDM) technology, parallel frequency mixing using a single photonic mixer becomes possible, which can dramatically reduce the system complexity and cost. Figure 2c shows a photonics-based microwave mixer, in which a 20-GHz RF and a 19-GHz LO are combined and introduced to the mixer. The electrical spectrum of the output signal is depicted in Figure 2d. Only the desired frequency component at 1 GHz is obtained, and all the unwanted frequency components are removed, which may enable a frequency conversion with a broad instantaneous bandwidth. As can be seen from **Figure 4**a, to guarantee sufficient spurious suppression and dynamic range, the typical wideband RF system usually use multiple narrow-band mixers,

Yifei Li received his bachelor's degree in optoelectronics engineering from the Huazhong University of Science and Technology, China, in 1996, and the M.S. and Ph.D. degrees in electrical engineering from the Drexel University in 2001 and 2003, respectively. He is currently a full professor in the UMassD. His research interests include microwave photonics, photonic integrated circuit, quantum electronics, theoretical laser physics, and high-power microwave devices.

Jianping Yao is a Distinguished University Professor and University Research Chair in Microwave Photonics in the University of Ottawa, Canada. He was an IEEE Distinguished Microwave Lecturer for 2013–2015. His research interests include microwave photonic signal generation and processing, integrated microwave photonics, fiber wireless communications, and microwave photonic sensing.

Shilong Pan is a professor and the executive director of the Key Laboratory of Radar Imaging and Microwave Photonics (issued by the Ministry of Education), Nanjing University of Aeronautics and Astronautics, China. His research has focused on microwave photonics, which includes optical generation and processing of microwave signals, analog photonic links, photonic microwave measurement, and integrated microwave photonics.

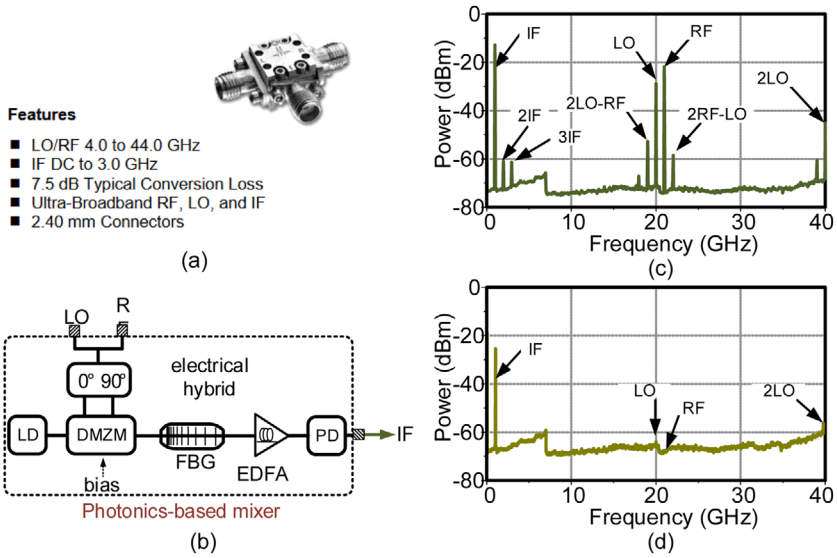

Figure 2. Example of a) a commercially-available broadband mixer (Marki M9-0440) and b) photonics-based microwave mixer, and c,d) the corresponding electrical spectra at the output when a 20-GHz RF and a 19-GHz LO are applied.

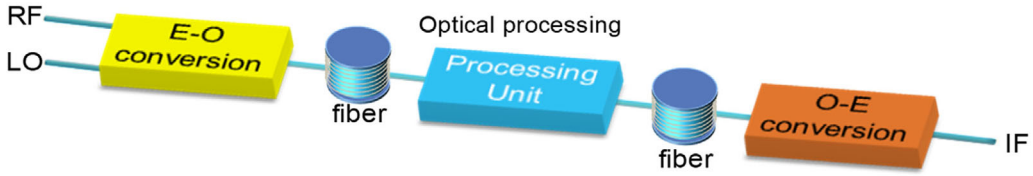

Figure 3. A generic system architecture of a photonics-based microwave mixer.

together with multiple electrical switches, preselector filters, and narrow-band microwave synthesizers, to process the received RF signals at different frequency bands.[7] Moreover, to realize high-performance image rejection, another stage of frequency mixing and image filter are also required. This architecture requires many high-performance RF filters, which are difficult to be integrated on a single chip. Besides, the filter banks will also result in considerable amplitude and phase ripples due to the voltage standing wave ratio (VSWR) interaction. Apparently, if wideband and high-performance (i.e., low mixing spurious, high dynamic range, and high image rejection ratio) photonics-based mixers are employed in the microwave systems to replace the conventional multi-stage narrow-band electrical mixers, narrow-band microwave synthesizers, switches, and filter banks are no more needed, and then the entire systems can be significantly simplified, as depicted in Figure 4b.

Based on this generic system architecture shown in Figure 3, numerous photonics-based microwave mixing approaches have been developed, to improve the conversion efficiency, dynamic range, mixing-spur suppression, mixing functionality, and polarization independence. In this article, we give a comprehensive overview of photonics-based microwave mixers reported over the past few years. The remainder of this article is organized as follows. Sections 2 and 3 describe all-optical and optoelectronic nonlinearities for microwave frequency conversion. Section 4 reviews the recent advances in photonics-based microwave frequency mixers associated with the improvements of conversion efficiency, conversion linearity, mixing spur suppression, mixing functionality, and polarization sensitivity. Section 5 describes several innovative RF systems with key performance improved (or new functionality enabled) by the photonics-based microwave mixing. The recent efforts in using photonic integrated circuits (PICs) to achieve photonics-based microwave mixing are reviewed in Section 6. In Section 7, a conclusion is made, and future prospects are discussed.

2. All-Optical Nonlinearities for Microwave Frequency Mixing

Since frequency conversion is primarily a nonlinear process, a straightforward way to achieve photonics-based microwave mixing is to find a device with strong nonlinear effects. Two main kinds of all-optical nonlinear devices can be employed, semiconductor optical devices and nonlinear optical fibers. The carrier density of a semiconductor device (or the refractive index of an optical fiber) would be changed by a strong pump light, and the variation of the carrier density (or refractive index) would, in turn, affect the other probe light transmission in the device. As a result, when a pump light modulated by an electrical RF signal and a probe light modulated by an electrical LO go through the semiconductor device, the pump light will change the carrier density of the semiconductor device. With the changed carrier density, the power (phase, or polarization state) of the probe light with

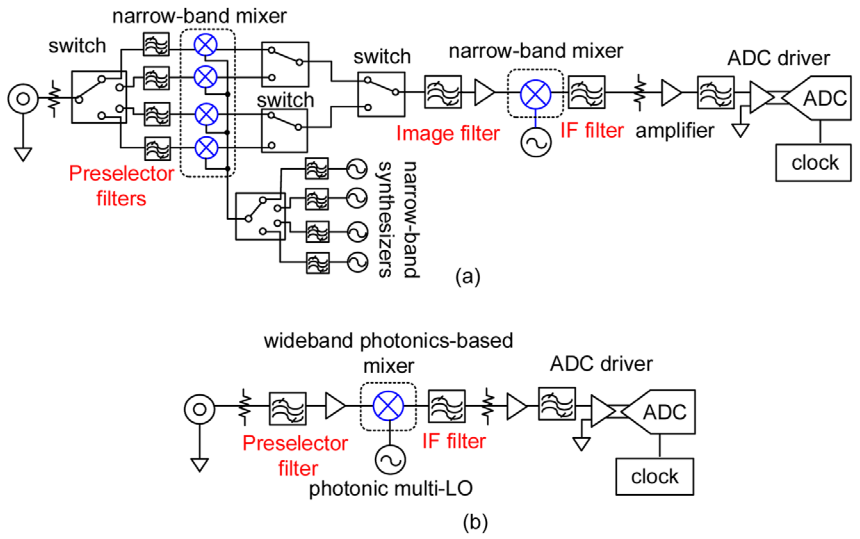

Figure 4. a) Typical microwave system architecture and b) the simplified system by using wideband photonics-based microwave mixers.

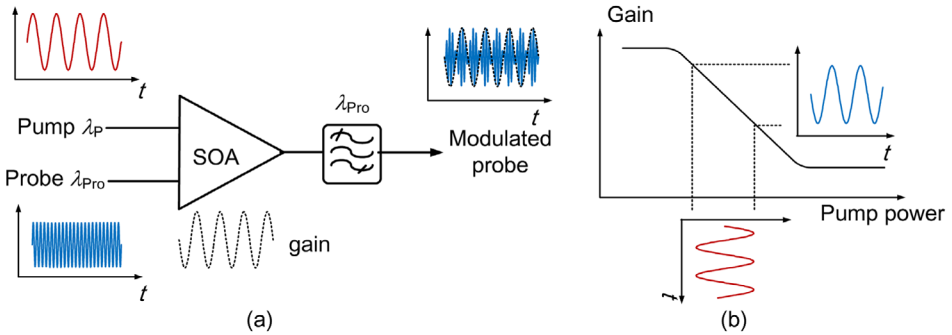

Figure 5. a) XGM effect in an SOA and b) the principle of the gain saturation effect.

be correspondingly changed. Therefore, the pump light and the probe light will influence each other and then new frequency components will be produced.

2.1. Photonics-Based Microwave Mixing Based on Nonlinearities in a Semiconductor Device

Semiconductor optical amplifiers (SOAs) are widely used to perform RF frequency conversion, as they are compact and potentially integratable with other optical devices.[8–10] Four main types of nonlinearities exist in an SOA, that is, cross-gain modulation (XGM), cross phase modulation (XPM), four-wave mixing (FWM), and cross polarization modulation (XPolM), which can be adopted to achieve the RF frequency mixing.

XGM is caused by the gain saturation of an SOA. A basic XGM scenario is shown in **Figure 5**a, in which a weak probe light (labeled as λ_{Pro}) and a strong modulated pump signal (labeled as λ_P) are injected into the SOA. Since, in general, the SOA has a homogeneously broadened gain spectrum, the change of the carrier density in the SOA will affect all of the input signals. That is to say, if the power of the pump signal is strong enough, the carriers are recombined with the holes in the SOA, leading to a large consumption of the carrier. As a result, the SOA will be saturated and the gain will be reduced. Under this condition, the probe light only has a very small or no gain, and thus the output power of the probe light will stay at a low level. In contrast, when the power of the pump light is low, the SOA will not be saturated and the gain is high. The probe light will be amplified and a strong probe light will be produced at the output of the SOA. The gain saturation effect of the SOA is illustrated in Figure 5b. Therefore, when the probe light is modulated by an LO signal with an angular frequency of ω_{LO} and the pump light is modulated by an RF/IF signal with an angular frequency of $\omega_{RF/IF}$, mixing products at frequencies of $|\omega_{RF/IF} \pm \omega_{LO}|$ would be produced.[11] One critical problem associated with the use of the XGM effect in an SOA is the relatively long carrier recovery time in the SOA, which leads to a small modulation bandwidth (typically lower than 10 GHz). If the frequency of the RF/IF signal carried by the pump light is too high, the frequency mixing will suffer from severe pattern effect and small extinction ratio. Even so, XGM-based frequency mixers are still considered a good solution because of the distinct advantages including simple configuration, high conversion efficiency, and integration capability.

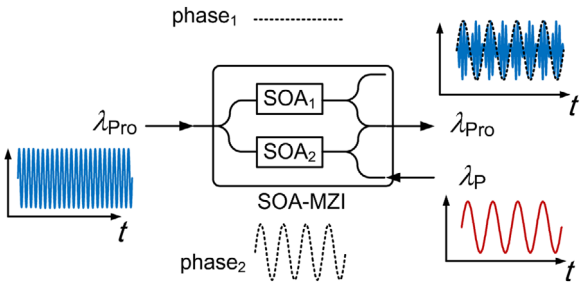

Figure 6. XPM effect in an SOA-MZI.

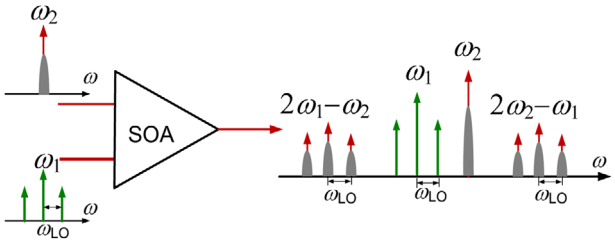

Figure 7. FWM effect in an SOA.

In addition, because the LO signal in the weak probe will not evidently affect the carrier density, its frequency could be very high. Therefore, an XGM-based frequency mixer is interesting for frequency upconversion. It should be noted that carrier-suppressed double sideband modulation is usually adopted to produce the probe light, which ensures a high conversion efficiency in an XGM-based frequency mixer.[12–18]

XPM is a phase-related nonlinearity, which results from the fact that the refractive index of an SOA's active region is dependent on the carrier density (or the material gain), that is, the phase and gain of an optical signal propagating through the SOA are coupled via gain saturation. Therefore, we can inject a strong pump light to introduce carrier density variation in the active region of an SOA, which changes the refractive index and then modifies the phase of a weak probe signal. It is worth noting that, since the XPM only changes the phase of an optical signal, which cannot be directly detected by a photodetector (PD), phase-modulation to amplitude-modulation (PM-to-AM) conversion is usually required before photodetection. Conventionally, PM-to-AM conversion is realized by placing two SOAs into an interferometric structure to form an SOA Mach–Zehnder interferometer (SOA-MZI),[19–22] as shown in **Figure 6**. As can be seen, if the probe light is modulated by an LO signal and the pump light carries an RF/IF modulated signal, microwave frequency mixing of the two signals can be realized via XPM. Although the modulation bandwidth is still limited by the carrier recovery time, XPM-based frequency mixers have many remarkable advantages as compared with the XGM-based ones. For example, the interferometric structure in the XPM-based mixer can have a large phase discrimination coefficient, so an improved extinction ratio can be achieved. Compared with XGM-based frequency mixers, the SOAs in XPM-based mixers do not need to work at deep gain-saturated conditions, so the requirement of a high pump power can be mitigated. In addition, the XPM-based scheme was also found to have excellent linearity and a high conversion efficiency.[19]

FWM is a coherent nonlinear process that occurs between two optical fields with the same polarization state in an SOA. When a strong pump light carrying an LO signal and a weak probe light carrying an IF/RF signal with the optical carrier frequencies of ω_1 and ω_2, respectively, are injected into the SOA, three main mechanisms can be used to generate FWM signals. When the frequency difference $\omega_2-\omega_1$ is small, the dominant mechanism is the carrier density modulation by the frequency beating between the input signals. This carrier density modulation is considered as an interband effect because it involves carrier-hole recombination between the material conduction and valence bands. The characteristic time of the process equals to the carrier lifetime, tens or hundreds of ps, so this mechanism will only manifest itself when $\omega_2-\omega_1$ is in the order of tens of GHz. If $\omega_2-\omega_1$ is greater than tens of GHz, the FWM signals are mainly generated by the effects called spectral hole burning (SHB) and carrier heating (CH). Caused by the injected pump signal, SHB creates a hole in the intraband carrier distribution, which effectively modulates the occupation probability of the carriers within a band and leads to fast gain modulation. CH is caused by stimulated emission and free carrier absorption. Both the SHB and CH have short characteristic times (in the order of 100 fs) due to the intraband effect. Through the above three mechanisms, as shown in **Figure 7**, new signals around angular frequencies of $2\omega_1-\omega_2$ and $2\omega_2-\omega_1$ will be generated. Meanwhile, the information carried by the probe light would be copied to the newly-generated components. Since frequency beating between any two FWM components will produce upconverted or downconverted microwave terms, frequency upconversion or downconversion is realized.[23–25] As compared with XGM and XPM, the nonlinear efficiency of FWM is much lower since FWM arises from high-order nonlinearity. Therefore, a microwave frequency mixer based on FWM usually has a relatively low conversion efficiency. Besides, to maximize the FWM effect, the pump and probe lights should have the identical polarization states,[23] which create difficulties if the RF signal is received remotely. Nevertheless, performing microwave frequency mixing based on FWM also has many useful features. FWM nonlinearity can produce a series of new frequency components, so more flexible frequency mixing can be realized by selecting different frequency components for photodetection.[23–25] More importantly, since the characteristic time of the FWM is very short (sub-ps level), large conversion bandwidths can be achieved.

Although most of the commercially available SOAs are claimed to be polarization-independent, birefringence still exists which results from the difference of the effective refractive indices along the TE and TM modes (due to the guiding properties of the amplifier waveguides). A very small index difference (of the order of 2×10^{-4} for a 2 mm long device at 1550 nm) is sufficiently high to induce a TE/TM phase shift of $\pi/2$. As a result, when a pump signal and a probe signal are injected into an SOA, the pump signal will change the birefringence in the SOA and thus change the polarization of the probe signal. This effect is known as nonlinear polarization rotation (NPR)[26,27] or XPolM.[28–30] Similar to the XPM, the XPolM-based all-optical frequency upconversion method has a good extinction ratio, but the cross-polarization-modulated signal cannot be

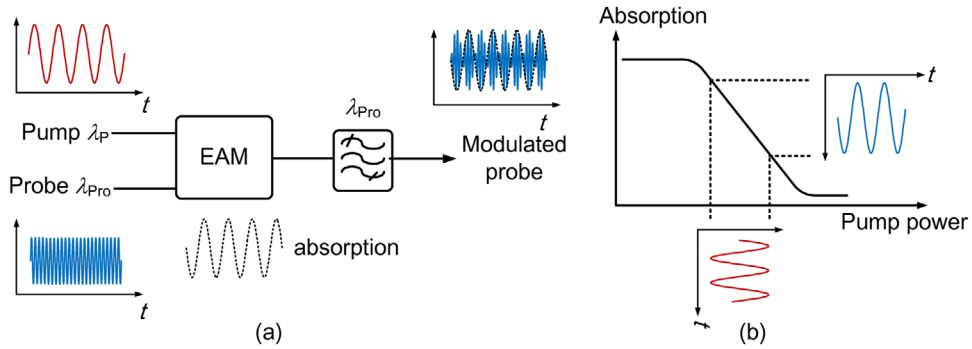

Figure 8. a) XAM effect in an EAM and b) principle of the absorption saturation effect.

Table 1. Microwave frequency conversion based on all-optical nonlinearities in semiconductor devices.

Device	Effect	Principle	Characteristic time	Advantage	Disadvantage
SOA	XGM	*Gain* is modulated by the pump light, and then changes the amplitude of the probe light	>10 ps	Simple configuration	Low extinction ratio, high distortion
	XPM	*Refractive index* is modulated by the pump light, and then changes the phase of the probe light	10–100 ps	Low required pump power, high extinction ratio	Requiring PM-to-AM conversion
	FWM	*Gain* is modulated by the frequency difference between the pump and probe light, and then generates new frequency components	<100 fs	Large conversion bandwidth	Low conversion efficiency, polarization dependent
	XPolM	*Birefringence* is modulated by the pump light, and then changes the polarization of the probe light	10–100 ps	High extinction ratio	Requiring PolM-to-AM conversion, polarization dependent
EAM	XAM	*Absorption* is modulated by the pump light, and then modulates the amplitude of the probe light	<10 ps	Simple configuration, large bandwidth	Low conversion efficiency, high pump power

detected directly either, so a polarizer should be placed at the output of the SOA to achieve polarization-modulation to amplitude-modulation (PolM-to-AM) conversion.[28]

In addition to the use of an SOA for mixing, an electroabsorption modulator (EAM) is another kind of all-optical nonlinear semiconductor device, of which the nonlinear cross-absorption modulation (XAM) can be applied to achieve frequency mixing. The principle of the XAM is shown in **Figure 8**, in which a pump signal and a weak probe signal are injected into the EAM. When the pump signal is weak, the absorption of the EAM will not be saturated, so both the pump and probe signal will be absorbed. On the other hand, if the pump signal is strong, the absorption of the EAM will be saturated, and an undiminished probe signal will be eventually output. Therefore, the probe light will be modulated by the pump, leading to the implementation of photonics-based microwave mixing if the pump and probe lights carry RF and LO signals, respectively.[31–33] The optical nonlinearities in an EAM have a smaller characteristic time than that of the XGM, XPM, and XPolM effects in the SOA, which is less than 10 ps. Therefore, a relatively larger conversion bandwidth can be realized. However, since XAM is based on the absorption effect, the conversion efficiency of the XAM-based mixer is low and a high optical pump power is usually required.

Table 1 summaries the approaches and characteristics of the microwave frequency mixing based on different all-optical nonlinearities in semiconductor devices. Recently, based on the simplest SOA and EAM, novel designed semiconductor devices like quantum dot SOA (QD-SOA),[34] reflective-SOA (RSOA),[35] SOA-EAM,[36] reflective-EAM (REAM),[37] SOA-REAM,[38] and RSOA-EAM,[39] were reported, which may also be applied to perform microwave frequency conversion.

2.2. Photonics-Based Microwave Mixing Based on Nonlinearities in Optical Fiber

In general, the nonlinearity of an optical fiber is due to the anharmonic motion of bound electrons under the influence of an applied field, which is determined by its *n*-th order susceptibility mathematically. The second-order susceptibility is nonzero only for the medium that lacks an inversion symmetry at the molecular level. As SiO_2 is a symmetric molecule, the second-order susceptibility is zero, so optical fibers do not normally exhibit second-order nonlinear effects. Therefore, the third-order nonlinear effects dominate the nonlinearity of the optical fiber, such as XPM, NPR, and FWM.[40] Based on the XPM, NPR, and

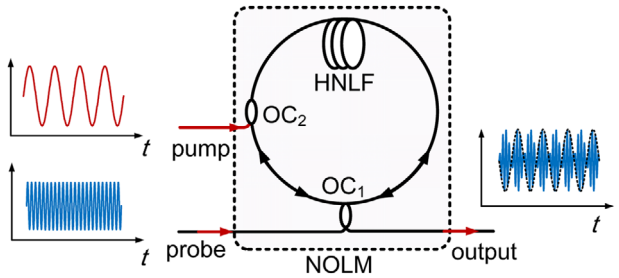

Figure 9. Frequency mixing based on XPM in a NOLM.

FWM in an optical fiber, especially in HNLF, microwave frequency mixing can be realized.

The XPM effect in an HNLF originates from the nonlinear refraction, a phenomenon referring to the intensity dependence of the refractive index. Mathematically, the refractive index of an optical fiber, in its simplest form, can be written as

$$n = n_1 + n_2|E|^2 \tag{4}$$

where n_1 is the linear part of the refractive index, and $n_2|E|^2$ is the nonlinear part which is dependent on the incoming electromagnetic field E and the Kerr coefficient n_2. When two optical signals with angular frequencies of ω_1 and ω_2 and optical fields of E_1 and E_2 propagate inside the HNLF, a nonlinear optical phase shift for the field at the angular frequency of ω_1 is given by[40]

$$\phi_{\mathrm{NL}} = n_2 k_0 L\left(|E_1|^2 + 2|E_2|^2\right) \tag{5}$$

where $k_0 = 2\pi/\lambda$ and L is the fiber length. As can be seen, the phase shift of one optical signal is determined by both the optical signal itself, that is, self-phase modulation (SPM) effect, and the other optical signal, that is, XPM effect, and the contribution of XPM to the nonlinear phase shift is twice that of SPM for equally intense optical fields. Therefore, when a strong optical RF signal and a weak optical LO is passed through the HNLF, the phase of the optical LO would be modulated by the optical RF signal via the XPM effect (SPM is ignored for $|E_1|<<|E_2|$), leading to frequency conversion. Unlike XPM in an SOA, of which the phase change is inevitably coupled with an amplitude variation, the XPM in an HNLF only changes the phase of the signal while the amplitude is unchanged. More importantly, since the XPM effect in an HNLF has no limitation of carrier recovery time, it responds very fast (fs-level), which can therefore be applied to high-frequency (e.g., 60 GHz or beyond) RF systems. However, PM-to-AM conversion is still required, which is usually performed by a nonlinear optical fiber loop mirror (NOLM).[41,42] The structure of an NOLM is shown in **Figure 9**. A probe light is split into two branches by an optical coupler (OC_1). One portion of the probe light goes through the HNLF along the clockwise direction, and the other portion propagates along the anti-clockwise direction. A strong pump light is injected into the loop by another optical coupler (OC_2), transmitting along the clockwise direction, to introduce different phase shifts to the clockwise and anti-clockwise probe lights via the XPM effect in the HNLF. The phase difference is proportional to the power of the pump light. Then, the probe lights from the two branches are recombined at OC_1, by which constructive or destructive interference is achieved to convert the phase change into intensity variation. Based on this principle, when an optical LO and an optical IF serve as a pump and probe light, respectively, frequency-converted components can be produced at the output of the NOLM after photodetection. One key problem associated with the XPM-based frequency mixing in an HNLF is the relatively low conversion efficiency due to the limited nonlinear coefficient of an optical fiber. Long optical fiber or large optical power is usually required. Recently, to reduce the length of the HNLF, highly nonlinear photonic crystal fiber (HNL-PCF) has been employed to replace a conventional HNLF in the NOLM to provide sufficiently high nonlinearity with a short length.[43]

The nonlinear optical phase shift is actually polarization dependent. For arbitrarily polarized light, the nonlinear part of the refractive index in Equation (4) due to the orthogonal electromagnetic fields E_x and E_y can be written as[40]

$$n_x = n_2 k_0\left(|E_x|^2 + \frac{2}{3}|E_y|^2\right) \qquad n_y = n_2 k_0\left(|E_y|^2 + \frac{2}{3}|E_x|^2\right) \tag{6}$$

As can be seen, the nonlinear phase shift caused by one polarization component is also influenced by the other polarization component, which leads to a nonlinear coupling between E_x and E_y. Generally, the nonlinear contributions of n_x and n_y are unequal, so a nonlinear birefringence is created which is dependent on both the intensity and polarization state of the incident light. Since the nonlinear birefringence usually leads to a rotation of the polarization ellipse, it is widely referred to as NPR effect. Based on the NPR effect, when a strong pump light and a probe light, modulated by an LO and an IF/RF signal, respectively, are injected into the HNLF along different polarization directions, the polarization state of the probe signal would be modulated by the pump light, and then frequency conversion can be realized after PolM-to-AM conversion and photodetection.[44] Since the response time of the NPR effect is typically at the sub-ps level, the NPR-based frequency conversion method can be applied to systems working at high-frequency bands.

The origin of the FWM in an optical fiber lies in the nonlinear response of bound electrons of a material to an electromagnetic field. It can occur if at least two different frequency components propagate together in the optical fiber. Assuming just two input frequency components ω_1 and ω_2 (with $\omega_2>\omega_1$), a refractive index modulation at the difference frequency occurs. When the refractive index modulation acts on ω_1, frequency components at $\omega_1\pm(\omega_2-\omega_1)$, which contains a new frequency component at $2\omega_1-\omega_2$, are produced, and when the modulation acts on ω_2, the frequencies of the generated signal would be $\omega_2\pm(\omega_2-\omega_1)$, which produces another new frequency component at $2\omega_2-\omega_1$. The information carried by the input signals would be copied to the newly-generated terms via the FWM effect. Although the FWM in the optical fiber is relatively weak and the polarization and wavelengths should be carefully designed to satisfy the phase-matching condition,[45] it is a feasible scheme to achieve photonics-based microwave frequency mixing, similar to the FWM-based mixers based on SOAs. For example, in ref. [46], eight probe lights with 2.5 Gbps baseband data, each are combined with an optical LO signal (40 GHz) and sent to a section of HNLF to generate an FWM signal. Then, the output signal is demultiplexed and detected at eight PDs. To obtain sufficiently

strong FWM, the power of the optical LO (pump light) is boosted to 14 dBm, and an additional backward Raman pump with a total power of 750 mW is launched into the system to increase the power of the converted signals. Again, to improve the conversion efficiency, specially designed optical fibers, for instance, bismuth oxide based fiber reported in ref. [47] can be used to enhance the FWM effect.

2.3. Photonics-Based Microwave Mixing Based on Nonlinearities in Other Materials and Devices

To improve the efficiency of the microwave frequency conversion, considerable attention is paid to find or develop new kinds of materials or devices that can provide strong nonlinearities without significantly increasing the complexity of the systems.[34,43,47] Recently, materials and devices like periodically poled lithium niobate (PPLN)[48] and As_2S_3 planar waveguide[49] were applied to realize high-efficiency photonics-based microwave frequency mixing since they possess strong second- or third-order nonlinearities. As the development of the material science and semiconductor integration technology progress, novel semiconductor devices can be explored, which may implement all-optical nonlinearity-based microwave frequency conversion with improved performance.

3. Optoelectronic Conversions for Microwave Frequency Mixing

Because E–O and O–E conversions are inherent nonlinear processes, microwave frequency mixing can also be implemented using E–O and O–E converters, such as directly modulated lasers, external electro-optic modulators, and PDs. As compared with all-optical nonlinearities, the optoelectronic nonlinearities are dependent not only on the properties of the material and device structure but also on many externally controlled parameters like bias current or voltage, and the conversion efficiency is usually several orders of magnitude stronger. Therefore, microwave frequency mixing based on E–O or O–E conversion has attracted significant interest recently. Different kinds of optoelectronic nonlinearities can be adopted to achieve microwave frequency mixing, such as the light–current (L–I) nonlinearity of laser diodes (LDs), the nonlinear electro-optic effects of external electro-optic modulators, and the square-law detection or capacitance/current–voltage (C/I–V) nonlinearity of PDs.

3.1. Photonics-Based Microwave Mixing Based on Direct Modulation

E–O conversion can be implemented by a directly modulated semiconductor LD. Direct modulation has the advantages of low cost and compact size, which is widely used in optical access networks. In general, both the amplitude and frequency modulation of the LD can be used to achieve photonics-based microwave mixing.

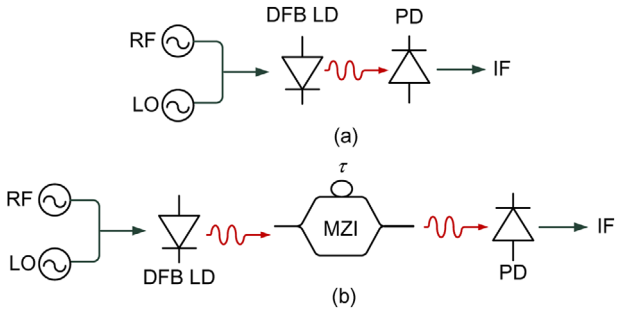

Figure 10. Microwave frequency conversion based on a) amplitude modulation and b) frequency modulation of a DFB.

Although the power of an LD output is expected to be linearly proportional to the input electrical signal, the real L–I curve of an LD is not strictly linear, especially when the LD is biased at the saturation region. Usually, we can expand the expression of the laser output in a Taylor series around the working point I_0.

$$P = \sum_{k=0}^{\infty} \frac{1}{k!} \frac{d^k P}{dI^k}\bigg|_{I_0} (I - I_0)^k \tag{7}$$

where I is the input current to the LD. When an electrical LO ($\sin\omega_{LO}t$) and an electrical RF ($\sin\omega_{RF}t$) signal are combined and applied to the LD, as shown in **Figure 10**a, the second-order term of Equation (7), that is, the dominant nonlinear term, can be expressed as

$$\begin{aligned} P &= \frac{1}{2} \frac{d^2 P}{dI^2}\bigg|_{I_0} (\sin\omega_{LO}t + \sin\omega_{RF}t)^2 \\ &= \frac{1}{2} \frac{d^2 P}{dI^2}\bigg|_{I_0} \left[1 - \frac{\cos(2\omega_{LO}t)}{2} - \frac{\cos(2\omega_{RF}t)}{2} \right. \\ &\quad \left. + \underbrace{\cos\{(\omega_{LO} - \omega_{RF})t\} - \cos\{(\omega_{LO} + \omega_{RF})t\}}_{\text{mixing components}} \right] \end{aligned} \tag{8}$$

As can be seen, due to the nonlinearity of the L–I curve of the diode, frequency-converted components are generated if the laser output is directed to a PD.[50–55]

In addition to the power of the LD that can be modulated by an electrical signal, the frequency of the LD can also be modulated by an electrical signal because the carrier density of the LD is closely related to the electrical signal applied to it. The carrier density variation then leads to the change in the refractive index of the gain medium, and therefore the cavity length of the LD. Thus, the oscillation frequency of the LD, which is determined by the cavity length, will be changed. When the LD serves as a frequency modulator, the output for the combined electrical LO and RF inputs can be expressed as[56]

$$E(t) = \cos(\omega_c t + \beta_{LO}\sin\omega_{LO}t + \beta_{RF}\sin\omega_{RF}t) \tag{9}$$

where ω_c is the angular frequency of the optical carrier, and $\beta_{LO/RF}$ is the frequency modulation index. Using the Bessel function expansion, Equation (9) can be rewritten as[56]

$$E(t) = \sum_l \sum_m J_l(\beta_{LO}) J_m(\beta_{RF}) \times \cos\left[\omega_c + (l\omega_{LO} + m\omega_{RF})\right] t \quad (10)$$

From Equation (10), intermodulation products at the frequency of $l\omega_{LO}+m\omega_{RF}$, including the desired frequency-converted terms ($l = m = 1$ or $l = -m = 1$), are produced in the optical domain. Similar to an XPM-based mixer using an SOA or HNLF, frequency modulation only changes the frequency while the amplitude (envelop) keeps unchanged, so the optical signal, as shown in Equation (10), cannot be directly detected by a PD. Frequency-modulation to amplitude-modulation (FM-AM) conversion is thus required, which is typically performed by inserting an unbalanced Mach–Zehnder interferometer between the LD and PD,[56] as shown in Figure 10b. A disadvantage of this approach is that the frequency-modulation noise of the laser can also be converted into an amplitude noise, which would result in a large noise figure. Unlike an amplitude-modulation-based frequency mixer, for which the LD should be biased in the nonlinear region of the *P–I* curve, the frequency modulation of the LD can be performed in the linear region.

Although direct modulation can achieve frequency mixing with a simple configuration and low cost, the bandwidth is usually limited by the frequency response of the semiconductor laser (typically lower than 20 GHz). Recently, wideband directly modulated LDs with a modulation bandwidth of 27,[57] 30,[58] and 44 GHz[59] have been reported, which can be applied to achieve high-frequency mixing. Another way to extend the operation bandwidth is to apply harmonic LO modulation using mode-locked lasers (MLLs),[60–63] on-chip optical frequency combs,[64,65] or injection of LO signals with large powers.[66] Taking the most widely used MLLs as an example, it is well known that passive Q-switching or mode-locking would occur if a saturable absorber is inserted into a laser cavity, which can generate a train of pulses with a repetition rate (denoted as f_{rep}) at microwave frequencies. Thus, an LO source with multiple frequency components equals to $n \times f_{rep}$ ($n \geq 1$) is internally generated by the self-oscillation in the MLL. Then, when the gain section of the laser is modulated by an RF signal, harmonic frequency mixing without using an external LO source would be implemented.[60,63] Similar photonics-based microwave mixing can also be performed if active mode-locking is introduced to a semiconductor laser.[61] For example, in ref. [61], a Fabry–Perot laser, which is monolithically integrated with an EAM, is actively mode-locked via loss modulation when an LO signal is injected into the EAM. With the gain section of the laser modulated by an IF signal, frequency upconversion with a conversion loss of lower than 2.7 dB was achieved.

3.2. Photonics-Based Microwave Mixing Based on External Modulation

External modulators to perform photonics-based microwave frequency conversion is generally based on the well-known electro-optic effects,[67] of which the most common one is the electrical field induced change of refractive indices (for instance, in a $LiNbO_3$ crystal). Due to the refractive index change, when

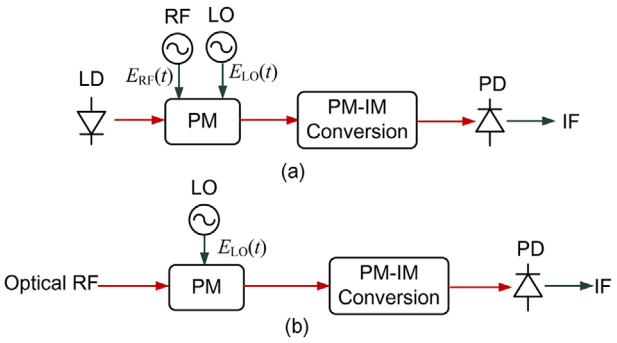

Figure 11. Microwave frequency conversion based on a phase modulator driven by an a) electrical or b) an optical RF signal.

CW light goes through the material, the phase of the optical signal will be modified according to the applied electrical signal, leading to external phase modulation. To realize photonics-based microwave mixing with phase modulation approaches, a straightforward way, as can be seen from **Figure 11**a, is to send an electrical LO and an electrical RF signal directly to a phase modulator. The optical carrier after phase modulation is given by[68]

$$E_{out}(t) = \exp\left(j\omega_c t + j\beta_{RF} \sin\omega_{RF} t + j\beta_{LO} \sin\omega_{LO} t\right) \quad (11)$$

Applying the Jacobi–Anger expansion, we obtain[68]

$$E_{out}(t) = \exp(j\omega_c t) \sum_l \sum_m J_l(\beta_{RF}) J_m(\beta_{LO}) \exp[j(l\omega_{RF} + m\omega_{LO})t] \quad (12)$$

After PM-to-AM conversion, the phase-modulated optical signal in Equation (11) is sent to a PD, by which microwave frequency mixing is realized through frequency beating between the frequency-converted sidebands (i.e., $l = m = 1$ or $l = -m = 1$) and the optical carrier or that between the 1st-order RF and LO sidebands. In practice, the RF signal might be delivered to the mixer through an optical fiber from a remote site, as can be seen from Figure 11b. In that case, photonics-based microwave mixing can still be implemented by directing an electrical LO to the phase modulator. For example, in ref. [68], the RF signal received from the remote site is modulated on an optical carrier at a phase modulator and the optical RF signal is sent to another phase modulator driven by the electrical LO. By using an optical notch filter to remove the optical carrier, PM-to-AM conversion is realized, which generates the frequency-converted components after photodetection. In ref. [69], the electrical RF signal is converted into an optical RF signal by a directly modulated LD, and fiber dispersion is used to implement the PM-to-AM conversion.

Although phase modulators are considered to have the advantages of low loss, high linearity, and free of bias drifting, the inevitable PM-to-AM conversion would bring significant limitations. For example, when the PM-to-AM conversion is realized by an optical filter, the operational frequency range of the microwave mixer will be restricted by the bandwidth of the optical filter. Besides, if the PM-to-AM conversion is implemented based on chromatic dispersion, a long fiber should be used, which increases the system loss and introduces a frequency-dependent sinusoidal power fading. An effective solution is to place two phase modulators into a Mach–Zehnder interferometer to form an

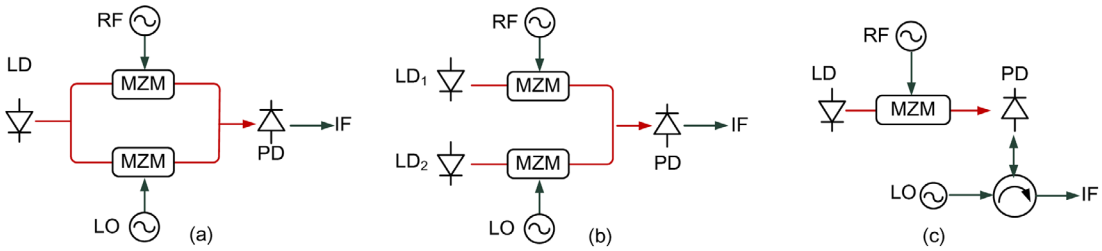

Figure 12. PD-based microwave frequency conversion driven by LO- and RF-modulated optical signals using a) a single LD and b) two LDs, and c) an optical RF signal and an electrical LO.

intensity modulator, which is known as a Mach–Zehnder modulator (MZM). If a voltage is applied to the electro-optic crystal, a phase shift difference is induced between the two arms of the interferometer. When the two arms are recombined, the phase difference can be converted into amplitude change, and thus amplitude modulation is realized. Similar to the configurations based on PMs shown in Figure 11, either an electrical RF signal[70–72] or an optical RF signal[73–75] can be used to drive an MZM-based microwave mixer.

Since external electro-optic modulators with > 60 GHz modulation bandwidth are commercially available, and those with > 100 GHz bandwidth have also been reported,[76–79] microwave frequency mixing based on external modulators are more preferred for RF systems operated at a high-frequency band. Besides, a directly modulated LD and an external electro-optic modulator sometimes can be applied together, especially for frequency-upconversion in which the low-cost directly modulated LD is modulated by low-frequency data and the wideband external modulator is modulated by a high-frequency LO.[80]

3.3. Photonics-Based Microwave Mixing Based on Optical-to-Electrical Conversion

In general, there are three types of mechanisms to implement microwave frequency mixing based on O–E conversion, as illustrated in **Figure 12**.

The square-law-detection nature of a PD is an ideal mechanism to realize photonics-based microwave mixing. According to Equation (2), frequency mixing is basically implemented by the second-order nonlinearity between the LO and RF/IF signals, which is presented as a square law operation on the input signals. It is well known that the main function of the PDs is to realize a square-law detection, so microwave frequency mixing can be easily implemented if the incident light contains the optical LO and RF/IF sidebands. Figure 12a shows a typical structure. An optical carrier is split into two branches, and in each branch, the optical carrier is modulated by the RF and LO signals in two independent modulators (MZMs, for example). The generated optical signals in each branch can be written as

$$\begin{aligned} E_{\mathrm{up}} &= J_0(\beta_{\mathrm{RF}})\exp(j\omega_c t) + J_1(\beta_{\mathrm{RF}})\exp[j(\omega_c+\omega_{\mathrm{RF}})t] \\ &\quad + J_1(\beta_{\mathrm{RF}})\exp[j(\omega_c-\omega_{\mathrm{RF}})t] \\ E_{\mathrm{down}} &= J_0(\beta_{\mathrm{LO}})\exp(j\omega_c t) + J_1(\beta_{\mathrm{LO}})\exp[j(\omega_c+\omega_{\mathrm{LO}})t] \\ &\quad + J_1(\beta_{\mathrm{LO}})\exp[j(\omega_c-\omega_{\mathrm{LO}})t] \end{aligned} \tag{13}$$

When the two optical signals in Equation (13) are combined and sent to a PD, frequency beating between the two optical signals is achieved, which is given by

$$\begin{aligned} i &\propto E_{\mathrm{up}}E_{\mathrm{down}}^{*} \\ &\propto [J_0(\beta_{\mathrm{RF}})J_1(\beta_{\mathrm{RF}}) + J_0(\beta_{\mathrm{LO}})J_1(\beta_{\mathrm{RF}})]\sin\omega_{\mathrm{RF}}t \\ &\quad + [J_0(\beta_{\mathrm{LO}})J_1(\beta_{\mathrm{LO}}) + J_0(\beta_{\mathrm{LO}})J_1(\beta_{\mathrm{RF}})]\sin\omega_{\mathrm{LO}}t \\ &\quad \underbrace{+J_1(\beta_{\mathrm{RF}})J_1(\beta_{\mathrm{LO}})[\sin(\omega_{\mathrm{RF}}+\omega_{\mathrm{LO}})t + \sin(\omega_{\mathrm{RF}}+\omega_{\mathrm{LO}})]}_{\text{Mixing components}} \end{aligned} \tag{14}$$

As can be seen from Equation (14), frequency mixing is realized by the square-law detection of the PD, rather than the nonlinearities of the modulators, so the modulators are expected to be biased at the quadrature transmission points to achieve high conversion linearity. Although the high IF/RF-to-LO isolation is still maintained in this method, it is hard to be applied to fiber remoting system because a common optical laser source should be used.

The responsivity modulation caused by the space-charge effect[81,82] or the photovoltaic effect,[83] by which the responsivity of the PD is modulated by a strong incident optical signal, is another mechanism to achieve photonics-based microwave mixing. When a PD with the modulated responsivity is employed to detect a second optical signal, mixing products with sum and difference frequencies are generated, as can be seen from Figure 12b. Unlike the method shown in Figure 12a, different LDs can be used for the RF and LO modulations, which can be applied to fiber-remoting applications. However, such kind of nonlinearity is relatively weak in a conventionally designed PD, so the PD design and operating regime should be carefully optimized to achieve high-efficiency microwave frequency conversion.

Microwave frequency mixing can also be realized based on the capacitance–voltage (C–V)[84,85] or current–voltage (I–V) nonlinearity[56,86] in a PD by leading an intensity-modulated optical RF signal to the optical port of the PD, and an electrical LO to the electrical port, as shown in Figure 12c. Taking the I–V nonlinearity as an example, the I–V relationship of a PD can be expressed as Taylor series by

$$I \cong F\left(V_{\mathrm{dc}}\right) + \left.\frac{dF(V)}{dV}\right|_{V_{\mathrm{dc}}}\Delta V + \frac{1}{2}\left.\frac{d^2F(V)}{dV^2}\right|_{V_{\mathrm{dc}}}\times\Delta V^2 + \cdots \tag{15}$$

where $V = V_{\mathrm{dc}} + V_{\mathrm{LO}} + V_{\mathrm{RF}}$ is the input signal, V_{dc} is the DC bias of the diode, and $V_{\mathrm{LO}} = \sin\omega_{\mathrm{LO}}t$ and $V_{\mathrm{RF}} = \sin\omega_{\mathrm{RF}}t$ are the input

Table 2. Photonics-based microwave frequency conversion based on optoelectronic conversions.

Method	Principle	Advantage	Disadvantage
E-O conversion	*Nonlinear* L–I *relationship* of the directly modulated LD	Low cost, simple configuration	Low bandwidth
	Frequency modulation of the directly modulated LD	Low cost, low bias requirement	Low bandwidth, requiring FM–AM conversion
	Electro-optic effects of the external modulators	Large bandwidth, high linearity	Large insertion loss, requiring PM-to-AM conversion
O–E conversion	*Square-law detection* of a PD driven by two optical signals with the same optical carrier	High conversion efficiency	Hard to achieve fiber remoting
	Responsivity modulation due to the space-charge or photovoltaic-effect of a PD driven by two optical signals with different optical carriers	Capability of achieving fiber remoting	Low efficiency
	C–V *or* I–V *nonlinearity* of a PD driven by an electrical LO and an optical RF signal	Simple configuration	Low LO bandwidth, and low port-to-port isolation

electrical LO and the modulated optical RF signals, respectively. Similar to Equation (8), considering the second-order term, Equation (15) can be modified as

$$\begin{aligned}\Delta I &\cong \frac{1}{2}\frac{d^2F(V)}{dV^2}\bigg|_{V_{dc}} \times \Delta V^2 \\ &= \frac{1}{2}\frac{d^2F(V)}{dV^2}\bigg|_{V_{dc}} \left(\sin\omega_{LO}t + \sin\omega_{RF}t\right)^2 \\ &= \frac{1}{2}\frac{d^2F(V)}{dV^2}\bigg|_{V_{dc}} \Big(\sin^2\omega_{LO}t + \sin^2\omega_{RF}t \\ &\quad + \underbrace{\cos(\omega_{LO}-\omega_{RF})t - \cos\left(\omega_{LO}+\omega_{RF}\right)t}_{\text{mixing components}}\Big)\end{aligned} \tag{16}$$

From Equation (16), we can see frequency mixing is realized. More recently, photonics-based microwave downconversion was implemented using PD sampling.[87] When an optical pulse train is injected into a uni-traveling-carrier (UTC) PD, a high-speed sampling switch is realized. If a weak optical RF signal is applied to the PD, it is gated by the switch. Frequency downconversion is therefore realized. Microwave frequency mixer in this category features simple configuration since both the functionalities of photodetection and frequency conversion are implemented by a single device. However, restricted by the bandwidth and the port isolation of the electrical circulator, the LO bandwidth of the frequency mixer is usually limited and the port-to-port isolation is low. **Table 2** summaries the methods and characteristics of microwave frequency mixing based on O–E conversions.

4. Properties of Photonics-Based Microwave Frequency Mixing

Similar to the electrical mixers, bandwidth, port-to-port isolation, conversion efficiency, conversion linearity (or dynamic range), and mixing functionality are key performance indicators for photonics-based microwave frequency mixers. Since the frequency conversion is implemented in the optical domain, the optical polarization sensitivity should also be taken into account when evaluating the performance of a photonics-based microwave frequency mixer. In this section, these important parameters will be introduced, and solutions to improve them are reviewed.

4.1. Conversion Efficiency

Conversion efficiency is used to characterize the loss (or gain) introduced by frequency conversion, which is defined as the ratio between the power of the converted component to that of the input RF/IF signal for frequency down- and up-conversion. Although electrical amplifiers can be inserted before or after a microwave mixer to amplify the converted signal, the noise figure and dynamic range of the entire system would be inevitably deteriorated. Therefore, it is highly desired that the conversion efficiency in the optical domain is high.

For microwave mixers based on all-optical nonlinearities, one promising way to increase the conversion efficiency is to use semiconductor devices or optical fibers with high nonlinearity. The nonlinearities of semiconductor devices can be enhanced based on novel materials or structures. For instance, a microwave mixer with enhanced conversion efficiency was achieved based on an ultra-nonlinear SOA (XN-SOA)[88] or InAs/InGaAs-based QD-SOA.[34] As_2S_3-based planar waveguides[49] and chalcogenide glass chips[89] were proven to have strong nonlinearity to achieve FWM, which allows realizing microwave mixing with high efficiency. To increase the nonlinearity of an optical fiber, we can apply specially designed (for instance, PCF[43]) or specially doped (for instance Bi-doped[47]) optical fiber.

For microwave mixers based on optoelectronic nonlinearity, optical carrier suppression coupled with optical amplification is widely adopted to increase the conversion efficiency. Taking a most common cascaded MZM-based microwave mixer as an example, the average optical power after the cascaded modulation can be expressed as

$$P_{O-avg} = \frac{t_{ff}^2}{4} G_{EDFA-1} P_{O-in} \tag{17}$$

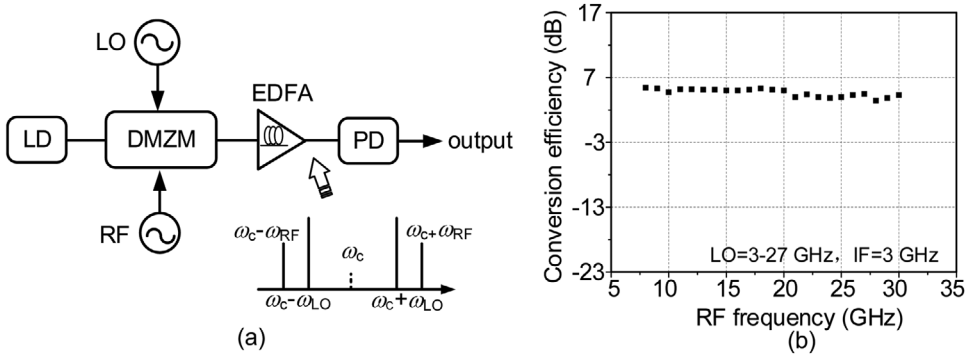

Figure 13. a) Schematic diagram of a microwave mixer based on a single DMZM, and b) the measured conversion efficiency.

and the conversion efficiency of the microwave mixer is written as[90]

$$\eta = \frac{t_{ff}^4}{16} G_{\text{EDFA}-1}^2 P_{\text{O}-\text{in}}^2 \Re^2 J_1^2(\beta_{\text{LO}}) \left(\frac{\pi}{V_\pi}\right)^2 R_{\text{in}} R_{\text{out}} \tag{18}$$

where $P_{\text{O-in}}$ is the optical power at the output of the LD, t_{ff} and V_π are the insertion loss and half-wave voltage of the MZM, respectively, $\Re$ is the responsivity of the PD, $G_{\text{EDFA-1}}$ is the gain of the erbium-doped fiber amplifier (EDFA), and R_{in} and R_{out} are modulator input resistance and photodiode load resistance, respectively. The frequency beating between the positive (or negative) 1st-order RF and LO sidebands contributes the most to the converted IF signal at the frequency of $(\omega_{\text{RF}}-\omega_{\text{LO}})$, and other optical components, especially the optical carrier, have no contributions to the frequency conversion while occupying most of the optical power. By suppressing the optical carrier before optical amplification, the conversion efficiency would be dramatically improved. With the optical carrier suppressed, the average output optical power and conversion efficiency become

$$P_{\text{O}-\text{avg}} = \frac{t_{ff}^2}{4} G_{\text{EDFA}-2} P_{\text{O}-\text{in}} \left[1 - J_0(\beta_{\text{RF}}) J_0(\beta_{\text{LO}})\right] \tag{19}$$

$$\eta = \frac{t_{ff}^2}{16} G_{\text{EDFA}-2}^2 P_{\text{O}-\text{in}}^2 \Re^2 J_1^2(\beta_{\text{LO}}) \left(\frac{\pi}{V_\pi}\right)^2 R_{\text{in}} R_{\text{out}} \tag{20}$$

where $G_{\text{EDFA-2}}$ is the gain of the EDFA. As compared with Equation (17), the relative large $J_0(\beta_{\text{RF}})$ and $J_0(\beta_{\text{LO}})$ (especially under small signal modulation condition) are removed from Equation (19). For optical amplifiers operating in saturation, $P_{\text{O-avg}}$ is almost the same, so the optical gain $G_{\text{EDFA-2}}$ would be much larger than $G_{\text{EDFA-1}}$. Because the conversion efficiency, as can be seen from Equations (18) and (20), is proportional to the square of the EDFA gain, an increased conversion efficiency is therefore realized. Based on this principle, carrier-suppressed modulation enabled by a dual-drive MZM (DMZM) was employed to achieve a high conversion efficiency microwave mixer.[71] **Figure 13**a illustrates the schematic diagram, in which an RF and an LO are applied to the two RF ports of the DMZM, respectively. By properly setting the bias voltage applied to the DMZM, the optical carrier will be significantly suppressed. After being amplified by an EDFA, the modulated signal is sent to a PD. Figure 13b shows the measured conversion efficiency. As can be seen, the conversion efficiency is about 6 dB, which is much larger than that of the cascaded-modulator-based microwave mixer (typically lower than −10 dB). Other optical carrier suppressed modulation methods, based on bias control of a bi-directional DMZM[90] or a dual-parallel MZM (DPMZM),[91,92] and notch filtering using a fiber Bragg grating (FBG)[93] or stimulated Brillouin scattering (SBS),[94] were also reported to achieve high conversion efficiency.

The conversion efficiency is also fundamentally dependent on the performance of E–O and O–E conversion, as can be seen from Equations (18) and (20). As a result, considerable efforts have been devoted to designing high-efficiency E–O and O–E conversion devices. For example, a 12 GHz $LiNbO_3$ MZM with a half-wave voltage of 1.5 V and an insertion loss of 8 dB[95] and a 40 GHz InP MZM with <7.5 dB loss and 1.5 V half-wave voltage[96] were reported to achieve high efficiency E–O conversion. In addition, to realize O–E conversion with high output power, a PD with a saturation photocurrent of 35 mA @ 20 GHz is commercially available and a PD with a saturation photocurrent of 95 mA @ 50 GHz was reported in the literature.[97]

4.2. Dynamic Range

The dynamic range of a microwave frequency mixer is a parameter that represents the highest and lowest power that a microwave frequency mixer can handle. The most common way to measure the dynamic range of a mixer is to use a two-tone test. In such a test, a closely spaced two-tone RF signal with angular frequencies of ω_{RF1} and ω_{RF2} and an LO with an angular frequency of ω_{LO} are applied to the mixer. Due to the nonlinearity of the system, various unwanted frequency components can be generated in addition to the desired IF components with angular frequencies of $(\omega_{\text{RF1}}-\omega_{\text{LO}})$ and $(\omega_{\text{RF2}}-\omega_{\text{LO}})$. The illustration of the output two-tone test spectrum is depicted in **Figure 14**a. Among all these unwanted frequency components, the third-order intermodulation (IMD3) components with frequencies of $(2\omega_{\text{RF1}}-\omega_{\text{RF2}}-\omega_{\text{LO}})$ and $(2\omega_{\text{RF2}}-\omega_{\text{RF1}}-\omega_{\text{LO}})$ located close to the IF frequencies cannot be filtered out by an electrical filter. Thus, the IMD3 is regarded as the main limiting factor of the dynamic range of a microwave mixer. Figure 14b shows the power of the IF and IMD3 components as a function of the input RF power. The IF power

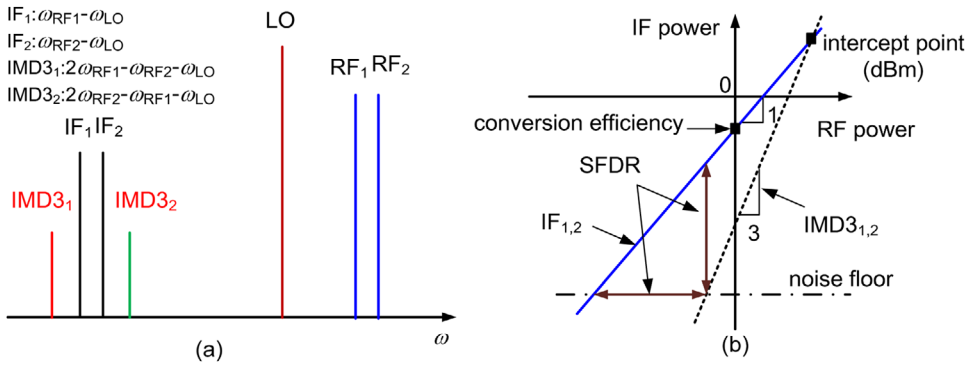

Figure 14. Illustrations of a) the output electrical spectrum for a typical two-tone test and b) the SFDR of a microwave mixer.

is increasing linearly with the increase in the RF power, which is plotted as the solid line with a slope of 1 in Figure 14b. The IMD3 power has a cubic relationship with the power of the input RF signal, which is plotted as the dashed line with a slope of 3. As a result, the power of the IMD3 increases more rapidly than that of the IF component when the input RF power increases. At a certain point, the IF and IMD3 components will have the same output power. The input RF power is named as the third-order input intercept point (IIP3), while the output IF power is called the third-order output intercept point (OIP3). Taking both the noise floor (shown as the dash–dotted line) and the nonlinearity into consideration, a parameter called spurious-free dynamic range (SFDR) is defined, which represents the minimum and maximum input power range corresponding to the IF power and the IMD3 power that are equal to the noise floor, respectively.

As can be seen from Figure 14b, the lowest power, which can also be defined as the sensitivity of the frequency conversion system, is determined by the noise floor of the system, and the highest power is determined by the nonlinear distortions of the system. Therefore, two strategies can be employed to increase the dynamic range of the conversion system. On the one hand, as the noise originates mainly from the shot noise at the PD, the thermal noise, the relative intensity noise (RIN) of the LD, and the amplified spontaneous emission (ASE) noise of the optical amplifier, low noise LDs and amplifiers can be applied to reduce the noise floor. For example, semiconductor lasers with a RIN below −160 dB Hz^{-1} have been developed,[98] which are now commercially available from Emcore Corporation,[99] and low-noise amplifiers (e.g., phase-sensitive amplifiers[100]) were also reported.[101] On the other hand, approaches to suppress nonlinear distortions can also be employed. A microwave frequency downconverter with an SFDR > 120 dB·$Hz^{2/3}$ has been proposed using a highly linear optical modulator,[102] and a low half-wave voltage and high linear quantum-well modulator developed by Li et al. led to a 28 dB improvement in distortion suppression ratio over that of a conventional photonics-based microwave frequency conversion link using $LiNbO_3$ MZMs.[103] Besides, by carefully setting the bias voltages of a DPMZM for RF signal modulation, an SFDR up to 127 dB·$Hz^{4/5}$ (IMD5 was the main distortion components in this condition, since the IMD3 components were significantly suppressed) was achieved when the IF frequency was around 150 MHz.[104] Since a phase modulator often exhibits higher linearity than an intensity modulator, a high dynamic range microwave downconverter can also be realized based on cascaded phase modulators together with optical filtering. By optimizing the power of the LO[68] or the optical filter response,[105] more than 10 dB enhancement of SFDR was achieved. In addition, digital signal post-processing can also be used to increase the SFDR of a microwave frequency conversion system.[106]

4.3. Mixing Spurs Suppression

Mixing spurs are the undesired frequency components at the output port of a microwave mixer. When an RF signal with a frequency of ω_{RF} and an LO with a frequency of ω_{LO} are applied to the mixer, frequency components expressed as $(n\omega_{RF}+m\omega_{LO})$ would be produced, which can be classified into three categories: 1) the wanted frequency-converted signals, when $n = 1$ and $m = 1$; 2) the LO and RF leakages, when $n = 1$ and $m = 0$ or $n = 0$ and $m = 1$; and 3) the harmonic mixing spurs, when n and m take other values. Because only the frequency beating between the +1st-order (or −1st-order) RF and LO sidebands generates the wanted frequency-converted components, an effective way to remove the unwanted mixing spurs (i.e., LO/RF leakages and harmonic mixing spurs) is to suppress the useless sidebands before photodetection.[107]

The RF and LO mixing spurs (leakages) are mainly caused by the frequency beating between the optical carrier and the 1st-order RF and LO sidebands, so the RF and LO leakages will be largely suppressed by removing the optical carrier. Other mixing spurs can be suppressed either in the optical domain[108–110] or in the electrical domain.[69,111–114] In the optical domain, sideband filtering is widely used. In ref. [108], the optical carrier was split into two branches. In the upper branch, the carrier was modulated by an RF signal and the +1st-order RF sideband was selected by an FBG. A similar operation was applied to the lower branch to select the +1st-order LO sideband. Then the two sidebands were combined by an optical coupler and sent to a balanced PD. As only the useful sidebands were detected by the balanced PD, other mixing spurs cannot be produced. Besides, since optical SSB modulation can naturally remove one of the 1st-order sidebands, mixing spur suppression would be simplified if optical SSB modulation was employed.[109,110] For example, in

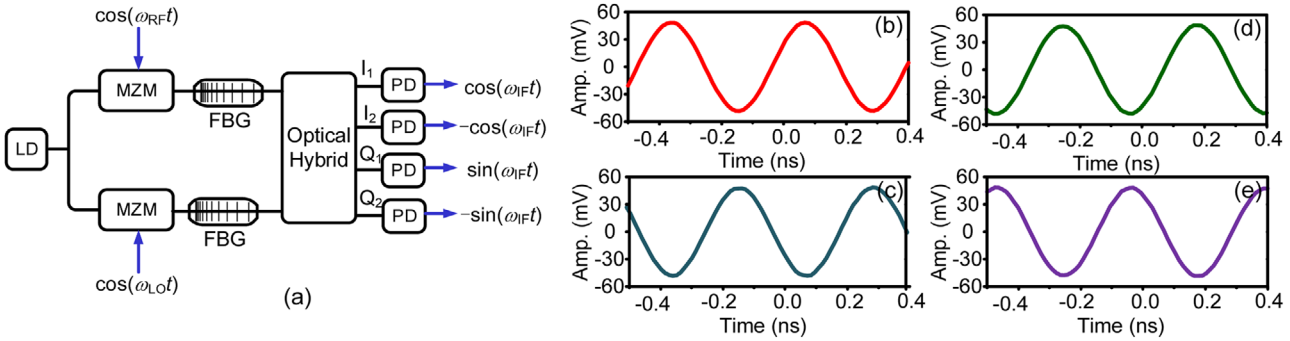

Figure 15. a) A reconfigurable microwave mixer based on an optical hybrid, and the waveforms of the b) I_1, c) I_2, d) Q_1, and e) Q_2 outputs.

ref. [109], a DMZM together with an electrical hybrid was used to perform the optical SSB modulation. Then an FBG was followed to suppress the optical carrier. In this way, only the +1st-order RF and LO sidebands were left. In the electrical domain, an electrical filter or photonic microwave filter can be employed to select the desired components. In ref. [69], a multi-wavelength laser source was used as the optical carrier. Since the multi-wavelength laser source together with fiber dispersion can function as a microwave bandpass filter, only the desired frequency-converted signals were selected. Similarly, in ref. 111–114, an optical comb source and an optical processor were employed to realize a reconfigurable photonic microwave filter to suppress the mixing spurs.

4.4. Mixing Functionalities

Most of the photonics-based microwave mixers can perform the simplest frequency conversion function, which is equivalent to single-ended frequency mixers. When a pair of LO sources with opposite or quadrature phase difference are introduced to two single-ended frequency mixers, double-balanced or I/Q mixing can be achieved. The pair of LO sources can be easily obtained by splitting an LO signal through an electrical 180- or 90-degree hybrid coupler,[115–120] a microwave photonic phase shifter,[121–128] or an optical hybrid.[129,130] The microwave photonic phase shifter can be realized by a DMZM,[121,123] a dual-polarization modulator,[120,122,124–126] or a DPMZM[127] followed by an optical filter. Based on the I/Q mixer, a mixer with the capability of image suppression for frequency downconversion or sideband suppression for frequency upconversion can be realized by connecting an electrical quadrature hybrid coupler to combine the output ports of the I/Q mixer.[131,132]

Recently, a reconfigurable microwave frequency mixer was reported,[130] with its configuration illustrated in **Figure 15**. In the scheme, an optical carrier, split into two branches, and modulated by an RF and an LO signal. In each branch, the +1st-order RF and LO sidebands are selected by an optical filter. The RF and LO sidebands are sent to an optical hybrid. The optical hybrid can introduce optical phase shifts to the LO sidebands by 0°, 90°, 180°, and 270°, corresponding to the four output ports of an optical hybrid, namely I_1, Q_1, I_2, and Q_2. For the in-phase (I_1 and I_2) or quadrature (Q_1 and Q_2) outputs, since a 180-degree phase shift exists, the converted IF components will be out-of-phase, by which a double-balanced frequency mixer can be obtained. For the quadrature outputs, due to the 90-degree phase difference, the converted IF signals will be in quadrature, which means an I/Q frequency mixer is achieved. When an electrical 90-degree hybrid is used to combine the two quadrature outputs of the I/Q mixer, image-reject mixing is realized.

4.5. Polarization Sensitivity

Since the photonics-based microwave frequency conversion is implemented in the optical domain, polarization sensitivity, a new property that is not considered in a conventional electrical mixer, should be taken into account. This parameter is important because most of the nonlinear optical devices and electro-optical modulators are polarization dependent. In the scenario of antenna remoting in which the antenna and the receiver are separated and connected by a long fiber, the polarization state of the modulated optical signal will be randomly changed due to environmental factors, leading to a fluctuation of the conversion efficiency. To solve this problem, active polarization control or dynamic digital signal processing should be incorporated into the transmitter or the receiver to maintain the polarization stability and to ensure the highest conversion efficiency, which makes the system complex, costly, and bulky.

Previously, a few polarization-insensitive photonics-based microwave frequency conversion approaches were proposed. In ref. [133], a polarization-insensitive SOA was applied to achieve frequency downconversion with small polarization dependence. In ref. [134], a polarization-insensitive frequency downconverter was reported by placing a $LiNbO_3$ phase modulator in a ring loop constructed by a polarization beam splitter and a Faraday rotator. More recently, a polarization-insensitive photonics-based microwave frequency converter based on two parallel intensity modulators and a balanced PD was proposed.[135] A 20 GHz RF signal was downconverted to a 1 GHz IF signal with polarization dependent loss of less than 0.06 dB.

It should be noted that, in most cases, people might not be able to find an approach that can achieve the best performances in all respects. For example, optical carrier suppression can achieve high conversion efficiency and large LO leakage suppression, but the dynamic range would be reduced. Therefore, the designer can choose the most suitable method according to the requirement of the system.

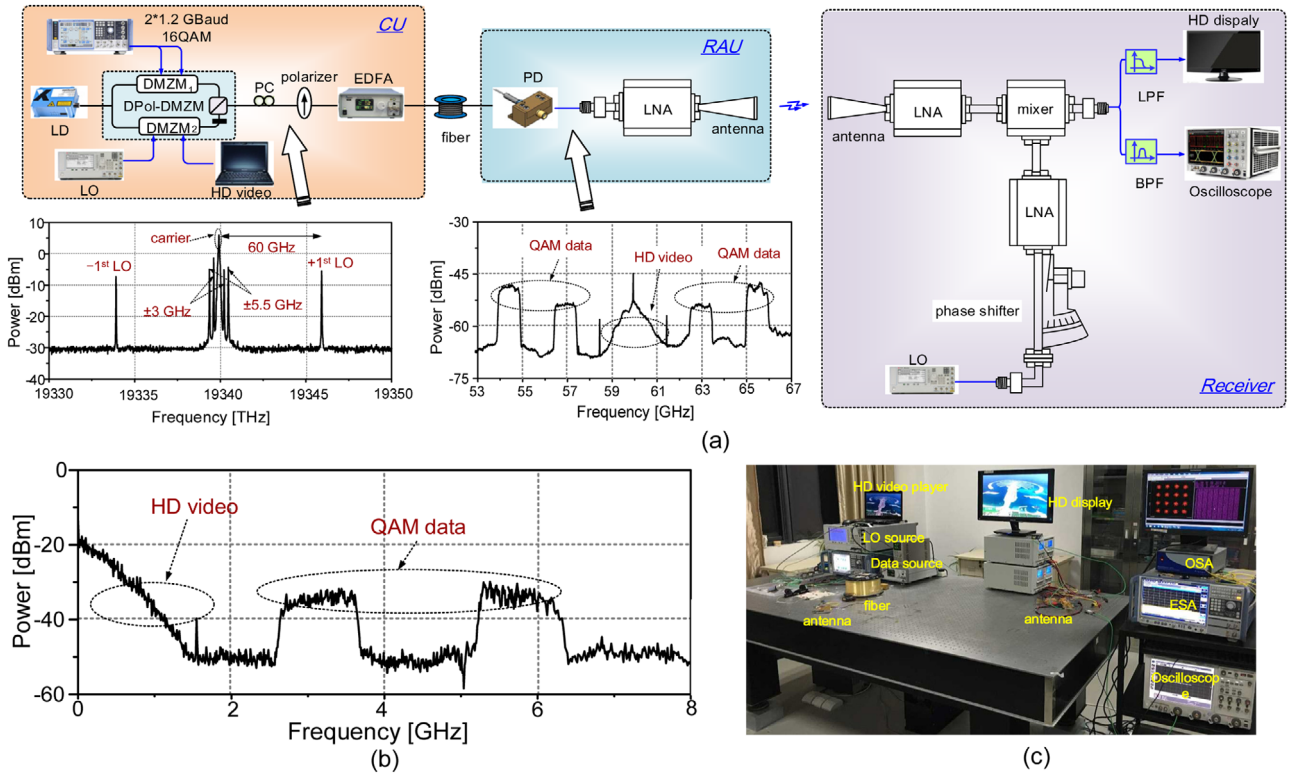

Figure 16. a) Experimental setup of a 60-GHz RoF system employing photonics-based microwave upconversion. b) Electrical spectrum of the down-converted signal. c) The photograph of the RoF system. Inset in (b): constellation diagram of the demodulated 16-QAM data.

5. Applications of Photonics-Based Microwave Frequency Mixing

A frequency mixer, as a basic component to construct an RF system, is essential in wireless communication, radar, EW, and microwave measurement systems. With the fast development of the photonics-based microwave frequency mixing, researchers began to incorporate the photonics-based microwave mixer into some experimental RF systems, including radio-over-fiber (RoF) communication systems, photonics-based radars, satellite repeaters, EW receivers, and many other innovative applications.

5.1. RoF Communication System

With the increasing demand for wireless data traffic, high-capacity, wide-coverage, ubiquitous-access, and low-latency wireless systems are being developed. Due to the rich spectrum resource in the higher-frequency band, millimeter-wave communication or even THz communication[136] becomes extremely attractive and is now tested for the next generation mobile communications. However, suffering from the high air link loss in the high frequency band, the wireless transmission range of the wireless services is usually restricted. To solve these problems, RoF systems at the millimeter-wave or even THz-wave band were proposed and extensively studied.[3,137–139] Frequency mixing is needed in both the transmitter and receiver of a RoF system. In the transmitter, microwave upconversion is usually used to upconvert the baseband data signal to the desired RF band, and in the receiver, the received RF signal should be downconverted to the baseband or IF band through frequency downconversion. Both the microwave mixers based on the nonlinear effects of an SOA or EAM,[16,20,23] and the wideband frequency conversion methods based on optoelectronic conversions[140–144] are widely used in literature to realize the frequency mixing for RoF communication systems. **Figure 16**a shows an example.[141] Two IF signals carrying 1.2 Gbaud 16 QAM data and baseband 1.5 Gb s^{-1} uncompressed 720P HD video data are mixed with a 60 GHz LO by a polarization-multiplexed microwave mixer. The optical spectrum of the modulated signal and electrical spectrum of the upconverted signal are shown as the inserts in Figure 16a. Figure 16b shows the electrical spectrum of the downconverted signal at the output of the mixer in the receiver. The designed data-rate of the RoF system is 11.8 Gb s^{-1}. The photograph of the experimental setup is presented in Figure 16c.

5.2. Radar Systems

Photonics-based microwave mixers can be applied to wideband RF transceivers[145] for radar applications. **Figure 17** shows an example of a photonic RF transceiver based on a microwave mixer using an MLL-based LO source. In the transmitter, the IF signal is modulated on each comb line of the MLL. Due to the frequency beating between different IF sidebands and the comb lines, multi-band frequency upconversion is realized after photodetection. By using electrical filters, RF signals with

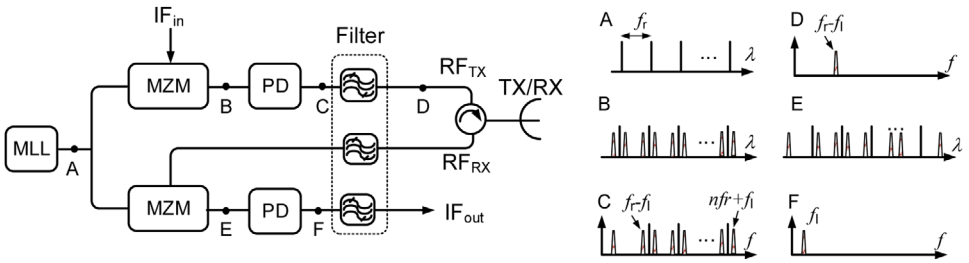

Figure 17. Radar transceiver based on photonics-based microwave frequency up- and down-conversion (left) and the optical and electrical spectra at different points of the transceiver (right).

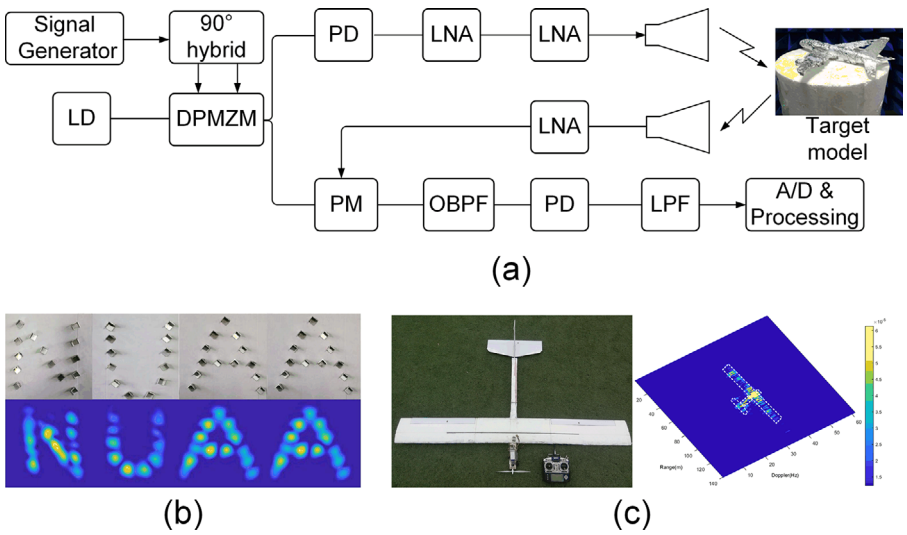

Figure 18. a) Experimental setup of the photonics-based ISAR system, b) imaging result of the letters of "NUAA," and c) picture and imaging result of a non-cooperative unmanned aerial vehicle.

the desired carrier frequencies can be selected for transmitting. In the receiver, the received RF signal is modulated on the comb lines from the same MLL. At a PD, the frequency beating between the RF-modulated optical sidebands and their nearest comb lines will be located in the IF band, and frequency downconversion is thus achieved. Based on this principle, the first fully photonics-based radar was developed.[5] In addition, radar systems with multiple functionalities can also be realized by using multi-band photonics-based microwave frequency up- and down-conversion. For instance, a dual-band (S and X band) photonics-based transceiver was demonstrated for the detection of moving targets[145] or cooperating/non-cooperating targets in the maritime scenario.[146] An MLL-based transceiver was also applied to simultaneously implement a dual-band (X and Ku band) photonics-based radar and a lidar.[147] In refs. [148–151], photonics-based inverse synthetic aperture radars (ISARs) for the imaging of non-cooperative object were reported. The typical experimental setup is shown in **Figure 18**a, and the obtained image is illustrated in Figures 18b and 18c, respectively. In this ISAR imaging radar system, photonics-based microwave mixing is applied to upconvert the IF linear-frequency modulated signal to the high-frequency band in the transmitter, and to realize de-chirping (i.e., frequency downconversion) in the receiver. A photonics-based multi-input-multi-output (MIMO) radar with high resolution and fast detection capability was proposed.[152,153] By using the wavelength division and multiplexing, multi-channel parallel photonics-based microwave mixing was realized, based on which a MIMO architecture was firstly introduced into the photonics-based radar system with improved radar performance and extended radar applications.[152] In addition, based on a photonic balanced I/Q frequency mixing in the receiver, a radar with the capability of interference suppression was realized.[154] More recently, as one of the most important modules, photonics-based microwave mixers were employed to realize 3D radars,[155] phased array radars,[156] and W-band radars.[157]

5.3. Satellite Repeater

Satellite communications have the advantages of seamless coverage of remote areas, reliable data relay for deep space exploration, and inherent multicasting and broadcasting capabilities. Frequency mixing is an essential part in a satellite repeater, since the uplink signal should be usually converted to have other carrier frequencies before broadcasting to other users. Since the working frequency of modern satellites must move from the low-frequency L band to the high-frequency Ka band or even

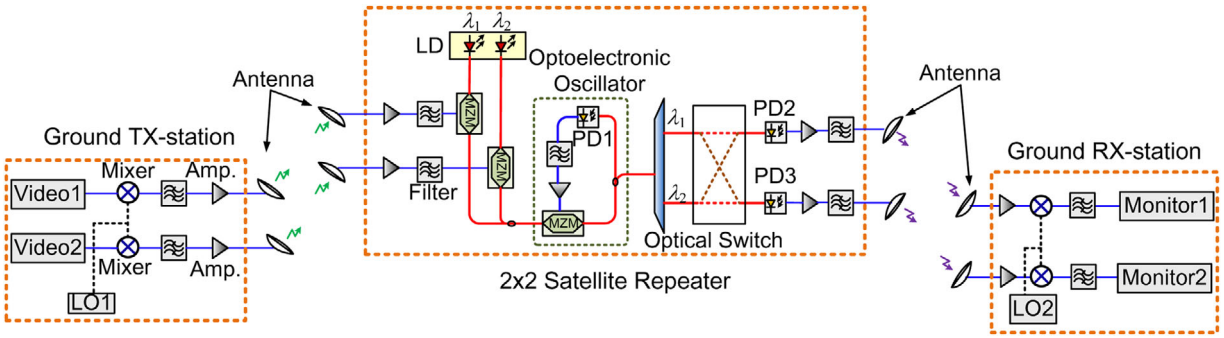

Figure 19. A 2 × 2 satellite repeater based on a photonics-based microwave mixer.

Q/V band, the frequency mixers inevitably face a lot of critical challenges, such as EMI, mass, volume, isolation, and power consumption, which are difficult to solve by the conventional electrical technologies.[158] Thanks to the numerous advantages brought by photonic technologies, photonics-based microwave mixers have attracted significant interest in satellite applications. The European Space Agency (ESA) is one of the pioneers in the research of satellite repeaters based on microwave frequency conversion in the optical domain.[159] Frequency mixing based on cascaded modulators was employed in their scheme, in which one modulator was driven by an electrical LO to produce an optical LO signal. When the optical LO was sent to the other modulator which was modulated by the RF signal, frequency downconversion was realized. An experimental demonstration of a 2 × 2 satellite repeater based on a microwave mixer was also performed in ref. [6] as shown in **Figure 19**.

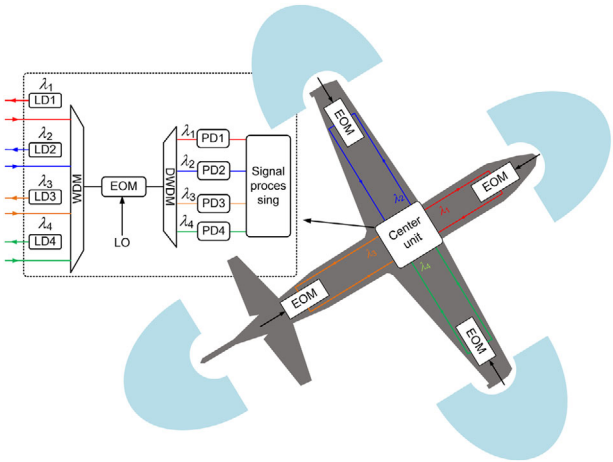

Figure 20. Block diagram of four-channel photonics-based microwave downconversion for avionic EW systems.

5.4. Electronic Warfare

The applications of photonics-based microwave mixers in electronic warfare date back to early 1990s when scientists in the field of defense technology predicted that warfighters and other military systems would soon face adversary systems that use signals outside the traditional EW spectrum. This creates a critical requirement of broadband RF equipment beyond the capabilities of conventional RF systems. Microwave photonic systems can implement multichannel frequency conversion with tens of GHz bandwidth, which are believed to provide EW systems with advanced performance.

Figure 20 shows a four-channel photonics-based microwave downconverter for an EW system demonstrated in an avionic platform.[160] In the photonics-based EW system, multiple optical carriers with different wavelengths (λ_i) are transmitted from the center unit to different remote sites of the airplane (i.e., nose, left wing, right wing, and empennage). In each remote site, an electro-optic modulator is placed to modulate the received RF signals onto the optical carrier. The RF-modulated optical signals from the remote modules are combined by a wavelength-division multiplexer and mixed with a common LO through another modulator. The converted optical signal is then demultiplexed into separated channels in which the downconverted IF signal is detected for each channel. Based on this parallel microwave frequency conversion, the complex and power-consuming processing and control modules are shifted from the remote sites to the center unit, which greatly reduces the SWaP of the system and makes the entire system easy to be scaled.

A channelization receiver is another widely adopted receiver architecture to accommodate the increasing bandwidth requirement of EW systems. The main idea of a channelizer is to slice a wideband RF signal into multiple narrow-band sub-channels to relieve the burden of signal processing in the electrical domain. Unlike a conventional RF channelizer which needs a number of strictly designed filters to slice the spectrum, an RF channelizer based on a microwave frequency mixer is realized by converting different portions of the RF signal to the same IF band by multiplying the received RF signal with a frequency-tunable or multiple-frequency LO source. For instance, in refs. [161, 162], a direct-conversion RF scanning channelizer employing photonics-based microwave downconversion was demonstrated. By scanning the frequency of the LO, different portions of the RF spectrum are downconverted to the same IF band in turn. The field trial results also demonstrated the high linearity and sensitivity of the photonic frequency-conversion-based channelizer.[163] In refs. [164–166], a parallel wideband RF channelizer based on a pair of coherent optical combs was also realized, in which the coherent optical combs are used as a

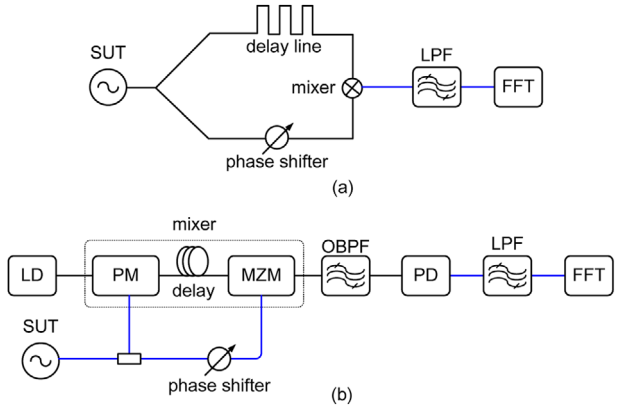

Figure 21. a) Principle of a phase noise measurement system based on a frequency discriminator, and b) the photonic demonstrator.

multi-LO source. The key advantage of RF channelizers employing photonics-based microwave mixers is that the resolution is significantly improved since the frequency of LO can be tuned at an Hz-level resolution. More importantly, by making use of the I/Q mixing and digital signal demodulation [164] or photonic image-reject mixing,[167–169] the spectrum aliasing problem, which makes the information unrecoverable caused by the square-law detection of the PD, can be effectively solved.

In fact, by making use of the advantages of wide bandwidth, low mixing spurs, low LO leakage, and high linearity offered by the photonics-based microwave mixers, multi-functional RF systems for communications, radar, sensing, and EW applications can be achieved in a unified platform, and a so-called "software-defined" radio system can be possibly implemented.[6,170]

5.5. Broadband Microwave Measurements

Photonics-based microwave mixers can be applied to a number of broadband microwave measurement systems,[171] such as phase noise measurements,[172–175] Doppler frequency shift measurements,[176–179] and angular-of-arrival measurements.[180,181] Here, we take a photonics-based phase noise measurement system as an example. Conventionally, the phase noise measurements are implemented by electronics. **Figure 21**a shows schematic diagram of an electrical frequency discriminator for low phase noise measurement. In the system, the frequency mixer functions as a phase detector to convert the phase difference between the two paths into a DC voltage. When the electrical mixers are replaced by their photonic counterparts, measuring the phase noise of a signal in a large frequency range can be achieved, with an example system presented in Figure 21b.[172] Based on the photonics-based microwave mixer, a 5–40 GHz phase noise measurement system with a noise floor of -137 dBc Hz^{-1} (10 GHz carrier at 10 kHz frequency offset) was realized. When a microwave photonic phase shifter is integrated into the microwave frequency mixing scheme to replace the electrical phase shifter, the phase noise measurement structure can be simplified further, and the bandwidth limitation caused by the electrical phase shifter can also be removed.[175] More recently, photonic I/Q modulation and digital phase demodulation was applied in the microwave phase noise measurement to simplify the calibration of the measurement system and to avoid the use of feedback loops and phase shifters,[182] which allowed achieving a measurement range of 5–35 GHz and a noise floor of -131 dBc Hz^{-1} at the offset frequency of 10 kHz.

6. PICs for Microwave Frequency Mixing

Although photonics-based microwave mixers have significant advantages as compared with their electrical counterparts, photonic-based mixers usually have relatively larger size, since most of them are implemented based on discrete optoelectronic components and devices. With the advancement of PIC technology,[183,184] microwave mixing based on PICs is gradually coming onto the stage and becoming a hot topic.

On the one hand, high-performance PIC-based key devices for microwave photonics, for example, lasers, modulators, and PDs, have been developed, which can be applied to build integrated microwave mixers with improved performance. Previously, low RIN and high-power LDs were fabricated to reduce the noise of the microwave photonic systems. For example, an InP-based slab-coupled waveguide laser with a RIN of -163 dB Hz^{-1} and an output power of 370 mW was reported.[185] To increase the linearity and electro-optic conversion efficiency, a 12 GHz dual-drive z-cut $LiNbO_3$ modulator with an ultra-low half-wave voltage of 1.4 V was developed.[95] Based on GaAs/AlGaAs substrate, an MZM was demonstrated to have a half-wave voltage of lower than 0.3 V.[186] A high-speed modulator with a half-wave voltage of 2 V was also fabricated based on InAlGaAs/InAlAs multi-quantum well structures.[187] New-material-based devices, such as graphene-,[188] thin-film-,[189] silicon-organic-,[190] plasmonic-,[191] polymer-,[192] $LiNbO_3$-on-insulator-,[193,194] and PZT-based[195] modulators were reported, which not only opens perspectives for the realization of electro-optical modulation, but also leads to significant breakthrough in terms of bandwidth, scalability, volume, and so on. Besides, to obtain high RF output power without external electrical amplification, a balanced PD with a 3-dB bandwidth of 8 GHz, a saturation current of 320 mA, and a maximum output RF power of 1.5 W was reported.[196] To maintain the high operational bandwidth of the microwave photonic system, an ultra-wideband PD with a bandwidth of >100 GHz has recently been developed to achieve wideband optical-to-electrical conversion.[197] Recently, a graphene-based PD[198,199] was also reported, which is shown in **Figure 22**. When an RF-modulated optical signal is launched into the graphene-based coplanar waveguide in the PD with an incident power of P_{opt}, and an electrical LO signal is applied to the PD as a bias voltage (V_{bias}), the obtained photocurrent is proportional to $P_{opt} \times V_{bias}$. Therefore, frequency-converted signals can thus be generated. In addition to the fabrication of high-performance optical-to-electrical and electrical-to-optical conversion devices, other functional components (e.g., SOAs, ring resonators) were also investigated to achieve high-performance microwave mixing. For instance, in ref. [200], a silicon torsional ring resonator was proposed to achieve microwave mixing, as presented in **Figure 23** . When a signal light carrying an RF signal is injected into the ring resonator, a mechanical frequency will be stimulated because of the effective index change induced by the pump

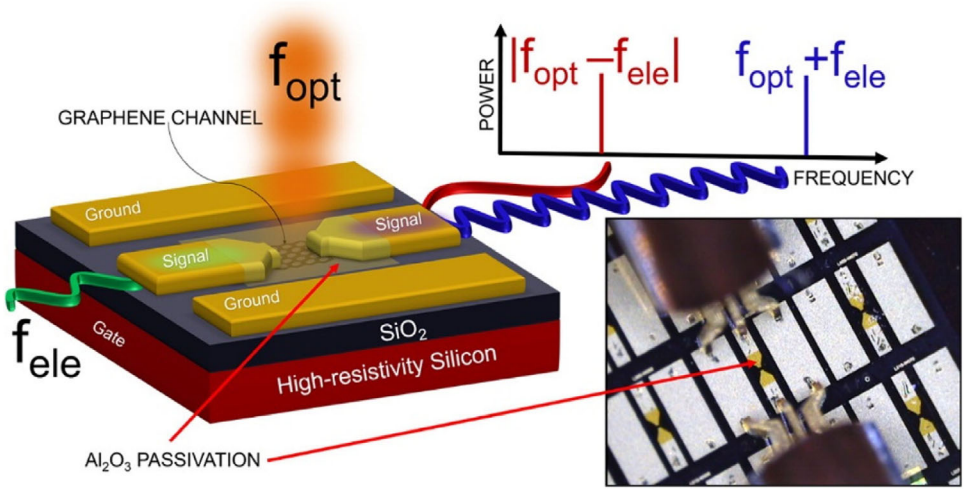

Figure 22. Integrated graphene-based optoelectronic mixer. Reproduced with permission.[199] Copyright 2016, American Chemical Society.

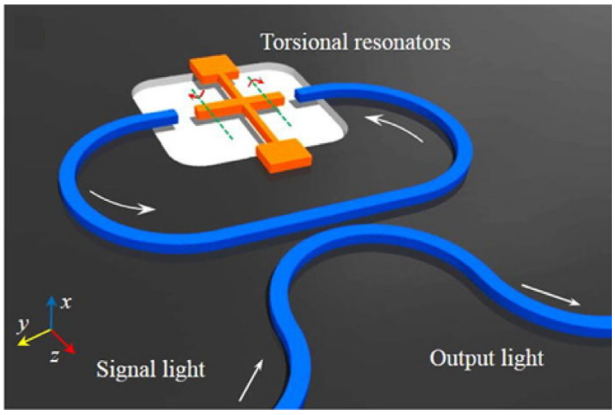

Figure 23. Photonics-based microwave mixer based on a torsional ring resonator. Reproduced with permission.[200] Copyright 2017, American Institute of Physics.

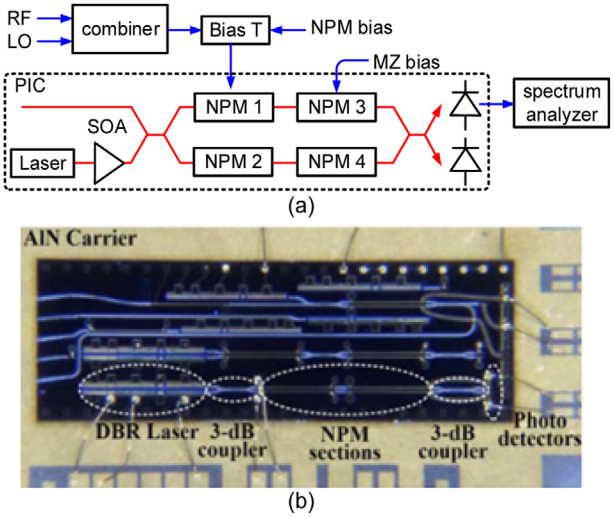

Figure 24. a) Experimental setup of the microwave mixer based on a fully-integrated circuit and b) the image of the PIC that is mounted on an AlN substrate. b) Reproduced with permission.[210] Copyright 2016, IEEE.

signal. Owing to the nonlinear coupling between the pump and mechanical frequencies, a frequency-converted signal can be obtained after photodetetion of the output light of the ring resonator. In ref. [201], an integrated conherent Kerr micro-comb source with a comb spacing of 48.9 GHz was fabricated on a silica glass platform. Based on this comb source, a photonic LO source was obtained and microwave frequency conversion over 40 GHz with a conversion efficiency of −6.8 dB was realized.

On the other hand, efforts are devoted to consolidating as many elements or units as possible on a single chip. For example, in ref. [202], a DFB laser was integrated with an MZM to achieve 100-Gbaud intensity modulation, and in ref. [203], quantum-well phase modulators were integrated with PDs on an InP substrate. When the chip in ref. [204] was used to perform frequency mixing, a conversion gain of −10 dB and an SFDR of 115 $dB \cdot Hz^{2/3}$ were achieved. Moreover, a quantum-well phase modulator integrated with an optical phase-locked loop module was also developed to achieve frequency mixing with an SFDR of larger than 120 $dB \cdot Hz^{2/3}$.[204,205] Recently, a similar phase modulator-based link was reported, which achieves a record SFDR of ≈129.3 $dB \cdot Hz^{2/3}$ with a bandwidth of 1 GHz.[206] An integrated silicon circuit consisting of two pairs of phase modulators and PDs[207,208] or a pair of EAMs[209] was applied to the transceiver to achieve photonics-based microwave up- and down-conversion. The measured SFDR was about 80 $dB \cdot Hz^{2/3}$.[208] A monolithic photonics-based microwave frequency conversion chip was first reported in ref. [210]. As can be seen from **Figure 24**, an LD, an SOA, four nonlinear phase modulators, two PDs, and other passive waveguides were all integrated into a single chip, which implements microwave mixing with an SFDR of ≈110 $dB \cdot Hz^{2/3}$. More recently, a research group from Ghent University and Antwerp Space developed a photonics-based microwave frequency mixing system with III-V-on-silicon photonic chip.[211] With the integrated MLL, MZM, and PD, five signals located at the different channels in the Ka-band (27.5–30 GHz) with 500 MHz bandwidth were downconverted to the L-band (1.5 GHz). These works demonstrate that photonics-based

Table 3. Promising PICs for microwave frequency mixing.

Year	Key components	Function	Key features	Material	Ref.
2007	MZM	MPL	Low V_{pi} (≈1.4 V)	$LiNbO_3$	[95]
2008	MZM	—	Low V_{pi} (<0.3 V)	GaAs/AlGaAs	[186]
2010	PM	MPL	High linearity	InP	[212]
2011	LD	—	Low RIN (−163 dB Hz^{-1}) and high power (370 mW)	InP	[185]
2011	MZM	—	Low V_{pi} (2 V)	InAlGaAs/InAlAs	[187]
2011	QW-PM/UTC-PD	MPL	High SFDR (>120 dB·$Hz^{2/3}$)	InP	[204]
2011	QW-PM/UTC-PD	Frequency mixer	High SFDR (125 dB·$Hz^{2/3}$)	InP	[205]
2012	EO modulator	—	High bandwidth (THz band)	Graphene	[188]
2012	QW-PM+UTC-PD	Frequency mixer	High SFDR (115 dB·$Hz^{2/3}$)	InP	[203]
2013	BPD	—	High output power (1.5 W) with 8-GHz bandwidth	InP/InGaAs	[196]
2015	EO modulator	—	High bandwidth and low V_{pi}	Polymer	[192]
2015	PD	Frequency mixer	Conversion loss of <35 dB	Graphene	[198]
2016	PPLN	Wavelength converter	Ultra-low loss (0.3 dB cm^{-1})	SiN thin film	[189]
2016	PD	Frequency mixer	RF bandwidth of 30 GHz	Silicon+ graphene	[199]
2016	Laser+PM+SOA+PD	Frequency mixer	Conversion loss of 9 dB and SFDR over 110 dB·$Hz^{2/3}$	InP	[210]
2016	Ring resonator	Frequency mixer	Using optomechanical effects	SOI	[200]
2017	IQ modulator	—	High bandwidth (100 GHz)	Silicon-organic	[190]
2017	MZM	—	High reliable beyond 130 °C	Ferroelectric plasmonic	[191]
2017	UTC-PD+RF amplifier	—	High bandwidth (100 GHz)	InP	[197]
2017	DFB+MZM	—	Large bandwidth (44 GHz) and low V_{pi} (2 V)	InP	[202]
2017	MLL+MZM+PD	Frequency mixer	K-band to Ka-band conversion	III/V	[211]
2017	PM+PD	Frequency mixer	Bandwidth: 2–10 GHz	SOI	[208]
2018	MZM	—	V_{pi} (1.4 V), bandwidth (100 GHz)	LNOI	[193]
2018	MZM	—	Bandwidth 30 GHz	PZT-SiN	[195]
2019	Comb	Frequency mixer	48.9-GHz spacing, 30.5 dBm pump power	Silica	[201]
2019	EAMs	Frequency mixer	Bandwidth: 7–26 GHz, SFDR = 82 dB·$Hz^{2/3}$	GeSi	[209]
2019	MZM	—	2.5 dB insertion loss, EO bandwidth > 70 GHz	LNOI	[194]
2019	PM	MPL	SFDR = 129.3 dB·$Hz^{2/3}$, 1 GHz bandwidth		[206]

MPL, microwave photonic link; LNOI, lithium niobite-on-insulator.

microwave mixers can have comparable size with the mature electrical mixers and competitive performance based on photonic integration. **Table 3** summarizes typical PICs covering key devices, sub-modules to systems-on-chip, for photonics-based microwave frequency conversion.

7. Discussion and Conclusion

In this article, after an introduction to the principle of photonics-based microwave mixing, we provide a comprehensive review of the latest advances in photonics-based microwave frequency mixing systems to improve the performance in terms of conversion efficiency, dynamic range, mixing spurs suppression, mixing functionality, and polarization dependence. Applications employing photonics-based microwave mixers were also reviewed.

Table 4 presents typical performance measures of the photonics-based microwave mixers and the conventional commercially available electronic mixers. It can be seen that for the photonics-based microwave mixers based on all-optical nonlinearities, the RF bandwidth can be very high thanks to the low characteristic time of the all-optical nonlinearities, especially the XPM[213] and XPolM[29] effect. Besides, due to the gain in the SOA, positive conversion efficiency is possible.[25,213] However, the SFDR is usually very low. For the microwave mixers based on optoelectronic conversions, the bandwidth is generally less than 40 GHz, limited mainly by the bandwidth of the electro-optic modulators. Although the conversion efficiency is usually negative because of the E–O/O–E conversion losses, positive conversion efficiency is achievable by optical amplification.[92] The SFDR of this kind of mixer is typically high, some of which is claimed to be higher than 120 dB·$Hz^{2/3}$.[104,130] Furthermore, when implementing the image-reject mixing, the image-reject ratio can be higher than 50 dB.[124,126,130] For the electronic mixers,[215–221] the RF bandwidths are usually limited to a single RF band, such as the K,[219] Ku,[221] and Ka[217] band. Only a few can achieve frequency mixing within multiple frequency bands.[215,216,218,220] The conversion efficiency is usually negative, but positive conversion efficiency value is possible when an electrical amplifier is integrated.[217] Besides, for the electronic image-reject mixer, the IF bandwidth is relatively narrow, and the image-reject ratio is lower than 23 dB.[216,217,220,221]

Table 4. Typical photonics- and electronic-based microwave mixers.

Structure	Type	RF BW [GHz]	IF BW [GHz]	CE [dB]	SFDR [dB·Hz$^{2/3}$]	IIP3 [dBm]	IRR [dB]	Ref.
SOA(XGM)	Photonics	0.2–10	<0.1	>−3	85.7	−5	—	[12]
SOA(XPM)	Photonics	47–71	1–14	7.5	72.5	NA	—	[213]
SOA(XPolM)	Photonics	31–75	0–15	−9	79.51	NA	—	[29]
SOA(FWM)	Photonics	20–45	<10	5.77	NA	NA	—	[25]
Single DPMZM	Photonics	2–16	<0.1	10.1	115	NA	—	[92]
DPMZM+MZM	Photonics	2–3.5	<0.15	≈−20	127	>10	—	[104]
MZMs+OH	Photonics	5.6–32	0–17	−15	120	>20	60	[130]
Single DPMZM	Photonics	10–40	0.1–1	<−5	108	≈20	50	[126]
Pol. Mods	Photonics	2–15	NA	−17.27	110.53	27	—	[214]
DPol-DMZM	Photonics	10–40	0–5	−20	NA	NA	60	[124]
PIC	Photonics	0–4	0–0.25	−9	>110	4	—	[210]
M9-0440	Electronic	4–40	0–3	−7.5	NA	<20	—	[215]
IRW-0618	Electronic	6–18	0.004–0.21	−7.5	NA	14	23	[216]
AR2640LI8C	Electronic	26–40	0.02–0.2	32	NA	13	23	[217]
M3608	Electronic	6.5–44	0–8	>−15	NA	20	—	[218]
FMMX1000	Electronic	16–26	0–8	−8	NA	19	—	[219]
ARM0618LC2A	Electronic	6–18	0.02–0.04	−24	NA	−9	18	[220]
IR-14-458	Electronic	14–16	0–0.02	−11	NA	NA	18	[221]

BW, bandwidth; CE, conversion efficiency; SFDR, spurious-free dynamic range; IIP3, third-order input intercept point; IRR, image-reject ratio; OH, optical hybrid.

Although the photonics-based mixers in Table 4 are not commercially available, which means that they lack essential optimization that the electronic mixers experience before being delivered to the market, the photonic microwave mixing technology still shows a number of advantages or potential advantages. The photonics-based mixers have a relatively large image-reject ratio, as can be directly seen from Table 4. Although the RF bandwidths of most of the reported photonics-based mixers are smaller than those in refs. [215,218], they can be easily increased to even hundreds of GHz by using wideband electro-optic modulators.[76–79,188,190,194,197] Since the frequency mixing is performed in the optical domain, long-distance transmission of the RF signal can be easily implemented via low-loss optical fiber, which is attractive for RF remoting applications. In addition, owing to the EMI immunity of photonics, parallel frequency mixing using a common photonic mixer can be achieved by using WDM technologies, so the complexity and cost of the entire system can be evidently reduced. The conversion efficiency of the photonics-based mixers is similar to that of the electronic mixers, and it can be increased by employing high-performance optoelectronic devices (e.g., high power LDs and PDs, low half-voltage modulators) or amplification,[92] which is widely used in the electronic mixers.[217] At this stage, most of the photonic-based frequency mixers have a relatively large size, low stability, and high power consumption, which is mainly due to the lower technology readiness level of the photonic integration technology. Fortunately, as the fast advancement in PICs, key optoelectronic devices (i.e., modulator, PD, etc.) with improved performances[194,196,205] and integrated photonics-based microwave mixers[209,210] were recently reported to reduce the size and the power consumption.

Future prospective may be focused on monolithically integrated PICs to achieve ultra-compact microwave mixers with superior performances competing with commercially available electrical mixers. These trends will make photonics-based microwave mixing a practical enabler for a wide range of applications in the near future.

Acknowledgements

The authors would like to thank Dr. D. Zhu, Mr. Q. S. Guo, and Mr. J. Z. Shi from the Key Laboratory of Radar Imaging and Microwave Photonics, Ministry of Education, Nanjing University of Aeronautics and Astronautics for their help and discussions during the paper preparation. This work was supported in part by the National Natural Science Foundation of China (61527820) and the Fundamental Research Funds for the Central Universities.

Conflict of Interest

The authors declare no conflict of interest.

Keywords

microwave frequency conversion, microwave photonics, photonic integrated circuits, radar

Received: December 18, 2018
Revised: October 14, 2019
Published online: November 28, 2019

[1] S. Maas, *IEEE Microw. Mag.* **2013**, *14*, 34.
[2] H. K. V. Lotsch, *IEEE Trans. Electron Devices* **1968**, *15*, 294.
[3] Z. Tang, S. Pan, *Photonic Netw. Commun.* **2016**, *32*, 179.

[4] L. Atzori, A. Iera, G. Morabito, *Comput. Netw.* **2010**, *54*, 2787.
[5] P. Ghelfi, F. Laghezza, F. Scotti, G. Serafino, A. Capria, S. Pinna, D. Onori, C. Porzi, M. Scaffardi, A. Malacarne, V. Vercesi, E. Lazzeri, F. Berizzi, A. Bogoni, *Nature* **2014**, *507*, 341.
[6] S. Pan, D. Zhu, S. Liu, K. Xu, Y. Dai, T. Wang, J. Liu, N. Zhu, Y. Xue, N. Liu, *IEEE Microw. Mag.* **2015**, *16*, 61.
[7] G. Cornwell, C. Gupta, Investigate wideband frequency converters, https://www.mwrf.com/systems/investigate-wideband-frequency-converters (accessed: April 2016).
[8] N. K. Dutta, Q. Wang, *Semiconductor Optical Amplifiers*, World Scientific, Singapore **2013**.
[9] M. J. Connelly, *Semiconductor Optical Amplifiers*, Springer Science & Business Media, Berlin **2007**.
[10] T. Durhuus, B. Mikkelsen, C. Joergensen, S. L. Danielsen, K. E. Stubkjaer, *J. Lightwave Technol.* **1996**, *14*, 942.
[11] W. Shieh, S. X. Yao, G. Lutes, L. Maleki, in *Proc. of Optical Fiber Communication Conf.*, OSA, Washington, DC **1997**, p. 263.
[12] C. Bohémond, T. Rampone, A. Sharaiha, *J. Lightwave Technol.* **2011**, *29*, 2402.
[13] Y. K. Seo, C. S. Choi, W. Y. Choi, *IEEE Photon. Technol. Lett.* **2002**, *14*, 1448.
[14] Y. K. Seo, J. H. Seo, W. Y. Choi, *IEEE Photon. Technol. Lett.* **2003**, *15*, 751.
[15] J. H. Seo, Y. K. Seo, W. Y. Choi, *IEEE Photon. Technol. Lett.* **2006**, *18*, 1389.
[16] H. J. Kim, J.-I. Song, *Opt. Express* **2009**, *17*, 9810.
[17] C. Bohémond, P. Morel, A. Sharaiha, T. Rampone, B. Pucel, *J. Lightwave Technol.* **2011**, *29*, 91.
[18] M. Park, J. I. Song, *Opt. Express* **2011**, *19*, 24499.
[19] H. J. Song, J. S. Lee, J. I. Song, *IEEE Photon. Technol. Lett.* **2004**, *16*, 593.
[20] H. J. Song, J. I. Song, *J. Lightwave Technol.* **2006**, *24*, 3028.
[21] T. Rampone, A. Lagrost, A. Sharaiha, A. Kabalan, *J. Lightwave Technol.* **2013**, *31*, 3597.
[22] H. Termos, T. Rampone, A. Sharaiha, A. Hamié, A. Alaeddine, *J. Lightwave Technol.* **2016**, *34*, 4688.
[23] H. J. Kim, J.-I. Song, H. J. Song, *Opt. Express* **2007**, *15*, 3384.
[24] W. Yang, M. Zhang, H. Han, L. Cai, P. Ye, *Opt. Eng.* **2008**, *47*, 075004.
[25] H. J. Kim, J. I. Song, *Opt. Express* **2012**, *20*, 8047.
[26] S. Fu, W. D. Zhong, P. Shum, Y. J. Wen, M. Tang, *IEEE Photon. Technol. Lett.* **2009**, *21*, 563.
[27] Y. Liu, M. T. Hill, E. Tangdiongga, H. d. Waardt, N. Calabretta, G. D. Khoe, H. J. S. Dorren, *IEEE Photon. Technol. Lett.* **2003**, *15*, 90.
[28] S. H. Lee, H. J. Kim, J. I. Song, *IEEE Photon. Technol. Lett.* **2013**, *25*, 1812.
[29] S. H. Lee, H.-J. Kim, J. I. Song, *Opt. Express* **2014**, *22*, 183.
[30] H. Soto, D. Erasme, G. Guekos, *IEEE Photon. Technol. Lett.* **1999**, *11*, 970.
[31] C. S. Park, C. K. Oh, C. G. Lee, D.-H. Kim, C. S. Park, *IEEE Photon. Technol. Lett.* **2005**, *17*, 1950.
[32] J. Yu, Z. Jia, G. K. Chang, *IEEE Photon. Technol. Lett.* **2005**, *17*, 2421.
[33] C. S. Park, Y. Guo, Y. K. Yeo, Y. Wang, L. C. Ong, S. Kato, *IEEE Photon. Technol. Lett.* **2008**, *20*, 557.
[34] M. Zajnulina, B. Lingnau, K. Ludge, *IEEE J. Sel. Top. Quantum Electron.* **2017**, *23*, 3000112.
[35] Z. Al-Qazwini, H. Kim, in *2012 17th Opto-Electronics and Communications Conf.*, IEEE, Piscataway, NJ **2012**, 921.
[36] D. Smith, I. Lealman, X. Chen, D. Moodie, P. Cannard, J. Dosanjh, L. Rivers, C. Ford, R. Cronin, T. Kerr, L. Johnston, R. Waller, R. Firth, A. Borghesani, R. Wyatt, A. Poustie, in *2009 35th European Conf. on Optical Communication*, IEEE, Piscataway, NJ **2009**, pp. 1–2.
[37] E. Hugues-Salas, R. P. Giddings, X. Q. Jin, Y. Hong, T. Quinlan, S. Walker, J. M. Tang, *Opt. Express* **2012**, *20*, 21089.
[38] A. Garreau, J. Decobert, C. Kazmierski, M. C. Cuisin, J. G. Provost, H. Sillard, F. Blache, D. Carpentier, J. Landreau, P. Chanclou, in *2006 Int. Conf. on Indium Phosphide and Related Materials Conf. Proc.*, IEEE, Piscataway, NJ **2006**, p. 168.
[39] B. Zhu, G. Chen, F. Zhang, R. Guo, D. Zhu, S. Pan, *IEEE Microw. Wirel. Compon.* **2014**, *24*, 275.
[40] R. W. Boyd, *Nonlinear Optics*, Elsevier, Amsterdam**2003**.
[41] N. J. Doran, D. Wood, *Opt. Lett.* **1988**, *13*, 56.
[42] A. Bogoni, M. Scaffardi, P. Ghelfi, L. Poti, *IEEE J. Sel. Top. Quantum Electron.* **2004**, *10*, 1115.
[43] B. Zsigri, C. Peucheret, M. D. Nielsen, P. Jeppesen, *IEEE Photon. Technol. Lett.* **2006**, *18*, 2290.
[44] W. Xue, K. Xu, J. Wu, J. Lin, *Opt. Eng.* **2007**, *46*, 060502.
[45] S. Song, C. T. Allen, K. R. Demarest, R. Hui, *J. Lightwave Technol.* **1999**, *17*, 2285.
[46] J. Yu, J. Gu, X. Liu, Z. Jia, G.-K. Chang, *IEEE Photon. Technol. Lett.* **2005**, *17*, 1986.
[47] J. Yu, Z. Dong, W. Jian, M. F. Huang, Z. Jia, X. Xin, G. K. Chang, T. Wang, in *2010 Conf. on Optical Fiber Communication/Collocated National Fiber Optic Engineers Conf. (OFC/NFOEC)*, IEEE, Piscataway, NJ **2010**, 1.
[48] C. Langrock, S. Kumar, J. E. McGeehan, A. E. Willner, M. M. Fejer, *J. Lightwave Technol.* **2006**, *24*, 2579.
[49] M. D. Pelusi, V. G. Ta'eed, M. R. E. Lamont, S. Madden, D. Y. Choi, B. Luther-Davies, B. J. Eggleton, *IEEE Photon. Technol. Lett.* **2007**, *19*, 1496.
[50] E. A. Avrutin, I. G. Thayne, D. A. Barrow, J. H. Marsh, E. L. Portnoi, V. B. Gorfinkel, in *IEE Colloquium on Towards Terabit Transmission*, IEEE, Piscataway, NJ **1995**, pp. 2/1–2/4.
[51] E. L. Portnoi, V. B. Gorfinkel, E. A. Avrutin, I. G. Thayne, D. A. Barrow, J. H. Marsh, S. Luryi, *IEEE J. Sel. Top. Quantum Electron.* **1995**, *1*, 451.
[52] E. L. Portnoi, G. B. Venus, A. A. Khazan, V. B. Gorfinkel, G. Kompa, E. A. Avrutin, I. G. Thayne, D. A. Barrow, J. H. Marsh, *Proc. SPIE Int. Soc. Opt. Eng.*, **1995**, *2426*, 304.
[53] S. B. Constant, Y. L. Guennec, G. Maury, N. Corrao, B. Cabon, *IEEE Photon. Technol. Lett.* **2008**, *20*, 120.
[54] S. B. Constant, Y. L. Guennec, G. Maury, M. Lourdiane, B. Cabon, *Microw. Opt. Techn. Lett.* **2008**, *50*, 1214.
[55] J. Lasri, M. Shtaif, G. Eisenstein, E. A. Avrutin, U. Koren, *J. Lightwave Technol.* **1998**, *16*, 443.
[56] G. Maury, A. Hilt, T. Berceli, B. Cabon, A. Vilcot, *IEEE Trans. Microwave Theory Techn.* **1997**, *45*, 1481.
[57] L. Yu, L. Guo, D. Lu, C. Ji, H. Wang, L. Zhao, *Chinese Opt. Lett.* **2015**, *13*, 051401.
[58] Z. Zhang, J. Liu, Y. Liu, J. Guo, H. Yuan, J. Bai, N. H. Zhu, in *Asia Communications and Photonics Conf. 2015*, OSA, Washington, DC **2015**, p. AM1B.3.
[59] N. Zhu, *Chinese Opt. Lett.* **2017**, *15*, 010002.
[60] B. A. Khawaja, M. J. Cryan, *IEEE Trans. Microwave Theory Techn.* **2010**, *58*, 3352.
[61] A. S. Daryoush, K. Sato, K. Horikawa, H. Ogawa, *IEEE Microw. Guided Wave Lett.* **1999**, *9*, 317.
[62] P. Acedo, H. Lamela, C. Roda, *IEEE Photon. Technol. Lett.* **2006**, *18*, 1888.
[63] J. M. Arnold, E. A. Avrutin, J. H. Marsh, E. L. Portnoi, in *Ultra–Wideband Short-Pulse Electromagnetics 4* (Eds: E. Heyman, B. Mandelbaum, J. Shiloh), **1998**, p. 229.
[64] P. Del'Haye, A. Schliesser, O. Arcizet, T. Wilken, R. Holzwarth, T. J. Kippenberg, *Nature* **2007**, *450*, 1214.
[65] Y. Okawachi, K. Saha, J. S. Levy, Y. H. Wen, M. Lipson, A. L. Gaeta, *Opt. Lett.* **2011**, *36*, 3398.
[66] H. Ogawa, Y. Kamiya, *IEEE Trans. Microwave Theory Techn.* **1991**, *39*, 2045.
[67] S. Datta, B. Das, *Appl. Phys. Lett.* **1990**, *56*, 665.

[68] V. R. Pagán, B. M. Haas, T. E. Murphy, *Opt. Express* **2011**, *19*, 883.
[69] Z. Fei, Y. Jianping, *IEEE Photon. Technol. Lett.* **2005**, *17*, 899.
[70] J. L. Corral, J. Marti, J. M. Fuster, *IEEE Trans. Microwave Theory Techn.* **2001**, *49*, 1968.
[71] Z. Tang, F. Zhang, D. Zhu, X. Zou, S. Pan, in *2013 IEEE International Topical Meeting on Microwave Photonics (MWP)*, IEEE, Piscataway, NJ **2013**, p. 150.
[72] B. H. Kolner, D. W. Dolfi, *Appl. Optics* **1987**, *26*, 3676.
[73] G. K. Gopalakrishnan, W. K. Burns, C. H. Bulmer, *IEEE Trans. Microwave Theory Techn.* **1993**, *41*, 2383.
[74] C. K. Sun, R. J. Orazi, S. A. Pappert, *IEEE Photon. Technol. Lett.* **1996**, *8*, 154.
[75] J. R. T. Logan, E. Gertel, in *SPIE Conf.*, **1995**, *2560*, 58.
[76] D. Chen, H. R. Fetterman, A. Chen, W. H. Steier, L. R. Dalton, W. Wang, Y. Shi, *Appl. Phys. Lett.* **1997**, *70*, 3335.
[77] L. Alloatti, R. Palmer, S. Diebold, K. P. Pahl, B. Chen, R. Dinu, M. Fournier, J.-M. Fedeli, T. Zwick, W. Freude, C. Koos, J. Leuthold, *Light Sci. Appl.* **2014**, *3*, e173.
[78] A. J. Mercante, S. Shi, P. Yao, L. Xie, R. M. Weikle, D. W. Prather, *Opt. Express* **2018**, *26*, 14810.
[79] M. Burla, C. Hoessbacher, W. Heni, C. Haffner, Y. Fedoryshyn, D. Werner, T. Watanabe, H. Massler, D. Elder, L. Dalton, arXiv:1901.00477, **2018**.
[80] J. Yao, G. Maury, Y. L. Guennec, B. Cabon, *IEEE Photon. Technol. Lett.* **2005**, *17*, 2427.
[81] T. Hoshida, M. Tsuchiya, *IEEE Photon. Technol. Lett.* **1998**, *10*, 860.
[82] M. Tsuchiya, T. Hoshida, *IEEE Trans. Microwave Theory Techn.* **1999**, *47*, 1342.
[83] S. A. Malyshev, B. A. Galwas, A. L. Chizh, J. Dawidczyk, V. F. Andrievski, *IEEE Trans. Microwave Theory Techn.* **2005**, *53*, 439.
[84] D. J. Roulston, *IEEE J. Solid-State Circuits* **1968**, *3*, 431.
[85] Y. Gu, D. Sun, J. Hu, S. Hu, N. Shi, X. Han, M. Zhao, *Opt. Laser Technol.* **2013**, *54*, 339.
[86] Q. Z. Liu, R. Davies, R. I. MacDonald, *IEEE Trans. Microwave Theory Techn.* **1995**, *43*, 2357.
[87] L. Xu, S. Jin, Y. Li, in *2016 IEEE Int. Topical Meeting on Microwave Photonics (MWP)*, IEEE, Piscataway, NJ **2016**, p. 114.
[88] Á. R. Criado, C. d. Dios, P. Acedo, *IEEE Photon. Technol. Lett.* **2012**, *24*, 1136.
[89] M. D. Pelusi, F. Luan, S. Madden, D. Y. Choi, D. A. Bulla, B. Luther-Davies, B. J. Eggleton, *IEEE Photon. Technol. Lett.* **2010**, *22*, 3.
[90] E. H. W. Chan, *Appl. Optics* **2014**, *53*, 1306.
[91] Y. Gao, A. Wen, H. Zhang, S. Xiang, H. Zhang, L. Zhao, L. Shang, *Opt. Commun.* **2014**, *321*, 11.
[92] E. H. W. Chan, R. A. Minasian, *J. Lightwave Technol.* **2012**, *30*, 3580.
[93] T. Jiang, S. Yu, Q. Xie, J. Li, W. Gu, *Opt. Lett.* **2014**, *39*, 4990.
[94] E. H. W. Chan, R. A. Minasian, *Opt. Lett.* **2013**, *38*, 5292.
[95] E. I. Ackerman, G. E. Betts, W. K. Burns, J. C. Campbell, C. H. Cox, N. Duan, J. L. Prince, M. D. Regan, H. V. Roussell, in *2007 IEEE/MTT-S Int. Microwave Symp.*, IEEE, Piscataway, NJ **2007**, p. 51.
[96] G. Letal, K. Prosyk, R. Millett, D. Macquistan, S. Paquet, O. Thibault-Maheu, J.-F. Gagné, P.-L. Fortin, R. Dowlatshahi, B. Rioux, T. SpringThorpe, M. Hisko, R. Ma, I. Woods, in *Optical Fiber Communication Conf.*, OSA, Washington, DC **2015**, p. Th4E.3.
[97] Q. Zhou, A. S. Cross, A. Beling, Y. Fu, Z. Lu, J. C. Campbell, *IEEE Photon. Technol. Lett.* **2013**, *25*, 907.
[98] R. W. Ridgway, C. L. Dohrman, J. A. Conway, *J. Lightwave Technol.* **2014**, *32*, 3428.
[99] Emcore Corporation, 1782 DWDM high power laser source, http://emcore.com/wp-content/uploads/2016/03/1782.pdf (accessed: October 2018).
[100] Z. Tong, C. Lundstrom, P. A. Andrekson, C. J. McKinstrie, M. Karlsson, D. J. Blessing, E. Tipsuwannakul, B. J. Puttnam, H. Toda, L. Gruner Nielsen, *Nat. Photon.* **2011**, *5*, 430.
[101] C. F. Ockeloen-Korppi, E. Damskägg, J. M. Pirkkalainen, T. T. Heikkilä, F. Massel, M. A. Sillanpää, *Phys. Rev. X* **2016**, *6*, 041024.
[102] C. Middleton, R. DeSalvo, in *Advanced Photonics*, OSA, Washington, DC, **2011**, p. SPMC3.
[103] L. Xu, S. Jin, Y. Li, *Opt. Express* **2016**, *24*, 8405.
[104] A. Altaqui, E. H. W. Chan, R. A. Minasian, *Appl. Optics* **2014**, *53*, 3687.
[105] P. Li, L. Yan, T. Zhou, W. Li, Z. Chen, W. Pan, B. Luo, *Opt. Lett.* **2014**, *39*, 2641.
[106] X. Liang, Y. Dai, F. Yin, X. Liang, J. Li, K. Xu, *Opt. Express* **2014**, *22*, 28247.
[107] Z. Tang, S. Pan, in *2015 14th Int. Conf. on Optical Communications and Networks (ICOCN)*, IEEE, Piscataway, NJ **2015**, p. 1.
[108] C. Middleton, A. Mast, R. DeSalvo, in *2012 IEEE Avionics, Fiber-Optics and Photonics Technology Conf.*, IEEE, Piscataway, NJ **2012**, p. 26.
[109] Z. Tang, S. Pan, in *2016 Optical Fiber Communications Conf. and Exhibition (OFC)*, **2016**, 1.
[110] Z. Tang, S. Pan, *IEEE Microw. Wirel. Compon.* **2016**, *26*, 67.
[111] D. Zou, X. Zheng, S. Li, H. Zhang, B. Zhou, *Opt. Lett.* **2014**, *39*, 3954.
[112] J. Wang, M. Chen, Y. Liang, H. Chen, S. Yang, S. Xie, in *2014 Int. Topical Meeting on Microwave Photonics (MWP) and the 2014 9th Asia-Pacific Microwave Photonics Conf. (APMP)*, IEEE, Piscataway, NJ **2014**, p. 222.
[113] J. Liao, X. Zheng, S. Li, H. Zhang, B. Zhou, *Opt. Lett.* **2014**, *39*, 6565.
[114] V. Torres-Company, D. E. Leaird, A. M. Weiner, *Opt. Lett.* **2012**, *37*, 3993.
[115] H. Ogawa, H. Kamitsuna, *IEEE Trans. Microwave Theory Techn.* **1992**, *40*, 2278.
[116] Z. Tang, S. Pan, in *2016 IEEE Int. Topical Meeting on Microwave Photonics (MWP)*, IEEE, Piscataway, NJ **2016**, p. 79.
[117] V. R. Pagán, T. E. Murphy, in *2014 IEEE Avionics, Fiber-Optics and Photonics Technology Conf. (AVFOP)*, IEEE, Piscataway, NJ **2014**, p. 13.
[118] C. Lu, W. Chen, J. F. Shiang, *IEEE Trans. Microwave Theory Techn.* **1997**, *45*, 1478.
[119] V. R. Pagán, T. E. Murphy, *Opt. Lett.* **2015**, *40*, 2481.
[120] Y. Gao, A. Wen, W. Jiang, Y. Fan, Y. He, D. Zhou, *IEEE Trans. Microwave Theory Techn.* **2018**, *66*, 4282.
[121] Z. Tang, S. Pan, in *2015 International Topical Meeting on Microwave Photonics (MWP)*, IEEE, Piscataway, NJ **2015**, pp. 1–4.
[122] Y. Gao, A. Wen, Z. Tu, W. Zhang, L. Lin, *Opt. Lett.* **2016**, *41*, 4484.
[123] T. Jiang, S. Yu, R. Wu, D. Wang, W. Gu, *Opt. Lett.* **2016**, *41*, 2640.
[124] Z. Tang, S. Pan, *J. Lightwave Technol.* **2016**, *34*, 4729.
[125] Z. Tang, S. Pan, in *2016 IEEE MTT-S Int. Microwave Symp. (IMS)*, IEEE, Piscataway, NJ **2016**, pp. 1–4.
[126] T. Jiang, R. Wu, S. Yu, D. Wang, W. Gu, *Opt. Express* **2017**, *25*, 4519.
[127] Y. Gao, A. Wen, W. Chen, X. Li, *Opt. Lett.* **2017**, *42*, 1105.
[128] W. Zhai, A. Wen, W. Zhang, Z. Tu, H. Zhang, Z. Xiu, *IEEE Photon. J.* **2018**, *10*, 1.
[129] S. R. O. Connor, M. C. Gross, M. L. Dennis, T. R. Clark, in *2009 Int. Topical Meeting on Microwave Photonics*, IEEE, Piscataway, NJ **2009**, pp. 1–3.
[130] Z. Tang, S. Pan, *IEEE Trans. Microwave Theory Techn.* **2016**, *64*, 3017.
[131] D. Zhu, S. Pan, *MDPI Photonics* **2018**, *5*, 6.
[132] D. Zhu, W. Chen, S. Pan, *Opt. Express* **2018**, *26*, 28022.
[133] R. Schnabel, U. Hilbk, T. Hermes, P. Meissner, C. Helmolt, K. Magari, F. Raub, W. Pieper, F. J. Westphal, R. Ludwig, L. Kuller, H. G. Weber, *IEEE Photon. Technol. Lett.* **1994**, *6*, 56.
[134] X. S. Yao, *IEEE Photon. Technol. Lett.* **2000**, *12*, 1382.
[135] X. Gu, S. Pan, Z. Tang, D. Zhu, R. Guo, Y. Zhao, *Opt. Lett.* **2013**, *38*, 2237.
[136] T. Nagatsuma, G. Ducournau, C. C. Renaud, *Nat. Photon.* **2016**, *10*, 371.

[137] D. Novak, R. B. Waterhouse, A. Nirmalathas, C. Lim, P. A. Gamage, T. R. Clark, M. L. Dennis, J. A. Nanzer, *IEEE J. Quantum Electron.* **2016**, *52*, 0600311.
[138] K. Xu, R. Wang, Y. Dai, F. Yin, J. Li, Y. Ji, J. Lin, *Photonics Res.* **2014**, *2*, B54.
[139] J. J. Vegas Olmos, I. Tafur Monroy, *J. Opt. Commun. Netw.* **2015**, *7*, B23.
[140] Z. Tang, S. Pan, *IEEE Photon. Technol. Lett.* **2016**, *28*, 852.
[141] Z. Tang, F. Zhang, S. Pan, *IEEE Photon. Technol. Lett.* **2018**, *30*, 1305.
[142] Z. Jia, J. Yu, G.-K. Chang, *IEEE Photon. Technol. Lett.* **2006**, *18*, 1726.
[143] J. V. Kerrebrouck, H. Li, S. Spiga, M. C. Amann, X. Yin, J. Bauwelinck, P. Demeester, G. Torfs, in *2018 Optical Fiber Communications Conf. and Exposition (OFC)*, IEEE, Piscataway, NJ **2018**, p. 1–3.
[144] K. V. Gasse, J. v. Kerrebrouck, A. Abbasi, G. Torfs, J. Bauwelinck, G. Roelkens, in *2017 Int.l Topical Meeting on Microwave Photonics (MWP)*, IEEE, Piscataway, NJ **2017**, pp. 1–4.
[145] F. Scotti, F. Laghezza, P. Ghelfi, A. Bogoni, *IEEE Trans. Microwave Theory Techn.* **2015**, *63*, 546.
[146] P. Ghelfi, F. Laghezza, F. Scotti, D. Onori, A. Bogoni, *J. Lightwave Technol.* **2016**, *34*, 500.
[147] F. Scotti, D. Onori, M. Scaffardi, E. Lazzeri, A. Bogoni, F. Laghezza, *IEEE Photon. Technol. Lett.* **2015**, *27*, 2268.
[148] F. Zhang, Q. Guo, S. Pan, *Sci. Rep.* **2017**, *7*, 13848.
[149] R. Li, W. Li, M. Ding, Z. Wen, Y. Li, L. Zhou, S. Yu, T. Xing, B. Gao, Y. Luan, *Opt. Express* **2017**, *25*, 14334.
[150] F. Zhang, Q. Guo, Y. Zhang, Y. Yao, P. Zhou, D. Zhu, S. Pan, *Chinese Opt. Letters* **2017**, *15*, 112801.
[151] S. Peng, S. Li, X. Xue, X. Xiao, D. Wu, X. Zheng, B. Zhou, *Opt. Express* **2018**, *26*, 1978.
[152] F. Zhang, B. Gao, S. Pan, *Opt. Express* **2018**, *26*, 17529.
[153] L. Lembo, P. Ghelfi, A. Bogoni, in *2018 Proc. Eur. Radar Conf.*, IEEE, Piscataway, NJ **2018**, p. 170.
[154] X. Ye, F. Zhang, Y. Yang, S. Pan, *Photon. Res.* **2019**, *7*, 265.
[155] X. Ye, F. Zhang, Y. Yang, D. Y. Zhu, S. Pan, *IEEE Access* **2019**, *7*, 79503.
[156] B. D. Gao, F. Z. Zhang, E. M. Zhao, D. C. Zhang, S. L. Pan, *Opt. Express* **2019**, *27*, 13194.
[157] N. Qian, W. W. Zou, S. T. Zhang, J. P. Chen, *Opt. Lett.* **2018**, *43*, 5869.
[158] J. V. Evans, A. Dissanayake, *Space Commun.* **1998**, *15*, 1.
[159] M. Sotom, B. Benazet, A. L. Kernec, M. Maignan, in *2009 35th European Conf. on Optical Communication*, IEEE, Piscataway, NJ **2009**, p. 1.
[160] M. E. Manka, in *2008 Int. Topical Meeting on Microwave Photonics jointly held with the 2008 Asia-Pacific Microwave Photonics Conf.*, IEEE, Piscataway, NJ **2008**, p. 275.
[161] D. Onori, F. Laghezza, F. Scotti, M. Bartocci, A. Zaccaron, A. Tafuto, A. Bogoni, A. Albertoni, P. Ghelfi, in *2016 IEEE MTT-S Int. Microwave Symp. (IMS)*, IEEE, Piscataway, NJ **2016**, p. 1–4.
[162] P. Ghelfi, F. Scotti, D. Onori, A. Bogoni, *IEEE J. Sel. Top. Quantum Electron.* **2019**, *25*, 8900209.
[163] D. Onori, F. Scotti, F. Laghezza, A. Bogoni, P. Ghelfi, M. Bartocci, A. Zacearon, A. Tafuto, A. Albertoni, in *2016 IEEE Int. Topical Meeting on Microwave Photonics (MWP)*, IEEE, Piscataway, NJ **2016**, p. 65.
[164] X. Xie, Y. Dai, K. Xu, J. Niu, R. Wang, L. Yan, J. Lin, *IEEE Photonics J.* **2012**, *4*, 1196.
[165] W. Hao, Y. Dai, Y. Zhou, F. Yin, J. Dai, J. Li, K. Xu, in *2016 IEEE Avionics and Vehicle Fiber-Optics and Photonics Conf. (AVFOP)*, IEEE, Piscataway, NJ **2016**, p. 183.
[166] W. Xu, D. Zhu, S. Pan, *Opt. Eng.* **2016**, *55*, 046106.
[167] Z. Tang, D. Zhu, S. Pan, *J. Lightwave Technol.* **2018**, *36*, 4219.
[168] C. X. Xie, D. Zhu, W. J. Chen, S. L. Pan, *IEEE Access*, **2019**, in press.
[169] W. J. Chen, D. Zhu, C. X. Xie, S. L. Pan, *Opt. Lett.* **2019**, *44*, 4052.
[170] M. Merritt, T. Brbooks, A. Stark, J. Rada, D. Nielsen, K. Davis, B. B. Yang, C. Ward, M. Quiggle, in *2016 IEEE Military Communications Conf.*, IEEE, Piscataway, NJ **2016**, p. 867.
[171] S. Pan, J. Yao, *J. Lightwave Technol.* **2016**, *35*, 3498.
[172] D. Zhu, F. Zhang, P. Zhou, S. Pan, *Opt. Lett.* **2015**, *40*, 1326.
[173] H. Peng, X. Peng, Y. Xu, C. Zhang, L. Zhu, W. Hu, Z. Chen, in *2016 15th Int. Conf. on Optical Communications and Networks (ICOCN)*, IEEE, Piscataway, NJ **2016**, pp. 1–3.
[174] W. Wang, J. G. Liu, H. Mei, W. Sun, N. Zhu, *J. Lightwave Technol.* **2016**, *34*, 3425.
[175] F. Zhang, D. Zhu, S. Pan, *Electron. Lett.* **2015**, *51*, 1272.
[176] B. Lu, W. Pan, X. Zou, X. Yan, L. Yan, B. Luo, *Opt. Lett.* **2015**, *40*, 2321.
[177] X. Zou, W. Li, B. Lu, W. Pan, L. Yan, L. Shao, *IEEE Trans. Microwave Theory Techn.* **2015**, *63*, 1421.
[178] B. Lu, W. Pan, X. Zou, Y. Pan, X. Liu, L. Yan, B. Luo, *J. Lightwave Technol.* **2016**, *34*, 4639.
[179] W. Chen, A. Wen, X. Li, Y. Gao, Y. Wang, S. Xiang, H. He, H. Zheng, *IEEE Photonics J.* **2017**, *9*, 1.
[180] X. Zou, W. Li, W. Pan, B. Luo, L. Yan, J. Yao, *Opt. Lett.* **2012**, *37*, 755.
[181] Z. Cao, Q. Wang, R. Lu, H. P. A. van den Boom, E. Tangdiongga, A. M. J. Koonen, *Opt. Lett.* **2014**, *39*, 1497.
[182] F. Zhang, J. Shi, Y. Zhang, D. Ben, L. Sun, S. Pan, *Opt. Lett.* **2018**, *43*, 5029.
[183] D. Marpaung, C. Roeloffzen, R. Heideman, A. Leinse, S. Sales, J. Capmany, *Laser Photon. Rev.* **2013**, *7*, 506.
[184] D. Marpaung, J. Yao, J. Capmany, *Nat. Photon.* **2019**, *13*, 80.
[185] P. W. Juodawlkis, J. J. Plant, W. Loh, L. J. Missaggia, F. J. O'Donnell, D. C. Oakley, A. Napoleone, J. Klamkin, J. T. Gopinath, D. J. Ripin, S. Gee, P. J. Delfyett, J. P. Donnelly, *IEEE J. Sel. Top. Quantum Electron.* **2011**, *17*, 1698.
[186] J. Shin, Y. C. Chang, N. Dagli, *Appl. Phys. Lett.* **2008**, *92*, 201103.
[187] S. Dogru, J. Shin, N. Dagli, in *24th IEEE Photonic Society Annual Meeting*, IEEE, Piscataway, NJ **2011**, p. 739.
[188] S. R. Berardi, Y. Rusen, K. M. M., F. Tian, T. Kristof, H. W. Sik, J. Debdeep, L. Lei, X. H. Grace, *Nat. Commun.* **2012**, *3*, 780.
[189] L. Chang, Y. Li, N. Volet, L. Wang, J. Peters, J. E. Bowers, *Optica* **2016**, *3*, 531.
[190] S. Wolf, H. Zwickel, C. Kieninger, Y. Kutuvantavida, M. Lauermann, J. Lutz, L. Altenhain, R. Schmid, W. Freude, C. Koos, S. Randel, in *Optical Fiber Communication Conf.*, OSA, Washington, DC **2017**, p. Th5C.1.
[191] A. Messner, F. Eltes, P. Ma, S. Abel, B. Baeuerle, A. Josten, W. Heni, D. Caimi, J. Fompeyrine, J. Leuthold, in *Optical Fiber Communication Conf.*, OSA, Washington, DC **2017**, p. Th5C.7.
[192] J. Liu, G. Xu, F. Liu, I. Kityk, X. Liu, Z. Zhen, *RSC Adv.* **2015**, *5*, 15784.
[193] C. Wang, M. Zhang, X. Chen, M. Bertrand, A. Shams-Ansari, S. Chandrasekhar, P. Winzer, M. Lončar, *Nature* **2018**, *562*, 101.
[194] M. He, M. Xu, Y. Ren, J. Jian, Z. Ruan, Y. Xu, S. Gao, S. Sun, X. Wen, L. Zhou, L. Liu, C. Guo, H. Chen, S. Yu, L. Liu, X. Cai, *Nat. Photon.* **2019**, *13*, 359.
[195] K. Alexander, J. P. George, J. Verbist, K. Neyts, B. Kuyken, D. Van Thourhout, J. Beeckman, *Nat. Commun.* **2018**, *9*, 3444.
[196] Q. Zhou, A. S. Cross, Y. Fu, A. Beling, B. M. Foley, P. E. Hopkins, J. C. Campbell, *IEEE Photonics J.* **2013**, *5*, 6800307.
[197] T. Umezawa, P. T. Dat, E. Hase, K. Kashima, A. Kanno, K. Akahane, A. Matsumoto, N. Yamamoto, T. Kawanishi, in *Optical Fiber Communication Conf.*, OSA, Washington, DC **2017**, p. W4B.2.
[198] X. Mao, C. Cheng, B. Huang, Z. Zhang, S. Gan, H. Chen, H. Chen, *IEEE Electron Device Lett.* **2015**, *36*, 253.
[199] A. Montanaro, S. Mzali, J.-P. Mazellier, O. Bezencenet, C. Larat, S. Molin, L. Morvan, P. Legagneux, D. Dolfi, B. Dlubak, P. Seneor, M.-B. Martin, S. Hofmann, J. Robertson, A. Centeno, A. Zurutuza, *Nano Lett.* **2016**, *16*, 2988.
[200] J. G. Huang, H. Cai, Y. D. Gu, L. K. Chin, J. H. Wu, T. N. Chen, Z. C. Yang, Y. L. Hao, A. Q. Liu, *Appl. Phys. Lett.* **2017**, *111*, 111102.

[201] J. Y. Wu, X. Xu, M. Tan, T. G. Nguyen, S. T. Chu, B. E. Little, R. Morandotti, A. Mitchell, D. J. Moss, in *CLEO: Science and Innovations*, OSA, Washington, DC **2019**, p. SF2N. 2.
[202] S. Lange, S. Wolf, J. Lutz, L. Altenhain, R. Schmid, R. Kaiser, C. Koos, S. Randel, M. Schell, in *Optical Fiber Communication Conf.*, OSA, Washington, DC **2017**, p. Th5C.5.
[203] S. Jin, A. Bhardwaj, P. Herczfeld, Y. Li, *IEEE Photon. Technol. Lett.*, **2012**, *24*, 1139.
[204] Y. Li, A. Bhardwaj, R. Wang, S. Jin, L. A. Coldren, J. E. Bowers, P. Herczfeld, *IEEE Photon. Technol. Lett.* **2011**, *23*, 1475.
[205] R. Wang, A. Bhardwaj, Y. Li, *IEEE Photon. Technol. Lett.* **2011**, *23*, 645.
[206] Y. F. Li, L. T. Xu, S. L. Jin, J. Rodriguez, T. Y. Sun, P. Herczfeld, *Optica* **2019**, *6*, 1078.
[207] Y. Li, L. Xu, P. Hcrczfeld, J. Rodriguez, in *2018 IEEE/MTT-S Int. Microwave Symp.*, IEEE, Piscataway, NJ **2018**, p. 1320.
[208] M. Chen, in *Optical Fiber Communication Conf.*, OSA, Washington, DC **2017**, p. W4B.3.
[209] K. V. Gasse, J. Verbist, H. Li, G. Torfs, J. Bauwelinck, G. Roelkens, *IEEE Photon. Technol. Lett.* **2019**, *31*, 181.
[210] S. Jin, L. Xu, V. Rosborough, J. Klamkin, Y. Li, *IEEE Photon. Technol. Lett.* **2016**, *28*, 1771.
[211] K. Van Gasse, Z. Wang, S. Uvin, B. De Deckere, J. Mariën, L. Thomassen, G. Roelkens, *CEAS Space J.* **2017**, *9*, 531.
[212] Y. Li, R. Wang, A. Bhardwaj, S. Ristic, J. Bowers, *IEEE Photon. Technol. Lett.* **2010**, *22*, 1340.
[213] D. H. Kim, J. Y. Lee, H.-J. Choi, J.-I. Song, *Opt. Express* **2016**, *24*, 20309.
[214] P. Li, W. Pan, X. Zou, S. Pan, B. Luo, L. Yan, *IEEE Photonics J.* **2015**, *7*, 1.
[215] Marki Microwave Inc., Double-balanced mixer M9-0444, https://www.markimicrowave.com/Assets/datasheets/M9-0444.pdf (accessed: November 2013).
[216] Marki Microwave Inc., Image reject double-balanced mixer IRW-0618, https://www.markimicrowave.com/Assets/datasheets/IRW-0618.pdf (accessed: March 2010).
[217] L3 Narda-Miteq Inc., Low-noise receive front end AR2640LI8A, https://nardamiteq.com/docs/AR2640LI8.PDF (accessed: August 2015).
[218] Advanced Microwave Inc., Double balance microwave Mixers M3608, http://www.advmic.com/m3x08.html (accessed: May 2019).
[219] Fairview Microwave Inc., Double balanced mixer FMMX1000, https://www.fairviewmicrowave.com/images/productPDF/FMMX1000.pdf (accessed: August 2016).
[220] L3 Narda-Miteq Inc., Image reject mixer ARM0618LC2A, https://nardamiteq.com/docs/MITEQ-ARM0618LC2.PDF (accessed: June 2006).
[221] Pulsar Microwave Corp., Image reject mixer IR-14-458, https://www.pulsarmicrowave.com/product/image_reject_mixer/IR-14-458 (accessed: June 2017).